THE ASTROPHYSICAL JOURNAL, 499:20–40, 1998 May 20

EVOLUTION OF STRUCTURE IN COLD DARK MATTER UNIVERSES

A. JENKINS,[1] C. S. FRENK,[1] F. R. PEARCE,[1,2] P. A. THOMAS,[2] J. M. COLBERG,[3] S. D. M. WHITE,[3] H. M. P. COUCHMAN,[4] J. A. PEACOCK,[5] G. EFSTATHIOU,[6] AND A. H. NELSON[7]
(THE VIRGO CONSORTIUM)

Received 1997 August 5; accepted 1998 January 2

ABSTRACT

We present an analysis of the clustering evolution of dark matter in four cold dark matter (CDM) cosmologies. We use a suite of high-resolution, 17 million particle, N-body simulations that sample volumes large enough to give clustering statistics with unprecedented accuracy. We investigate a flat model with $\Omega_0 = 0.3$, an open model also with $\Omega_0 = 0.3$, and two models with $\Omega = 1$, one with the standard CDM power spectrum and the other with the same power spectrum as the $\Omega_0 = 0.3$ models. In all cases, the amplitude of primordial fluctuations is set so that the models reproduce the observed abundance of rich galaxy clusters by the present day. We compute mass two-point correlation functions and power spectra over 3 orders of magnitude in spatial scale and find that in all of our simulations they differ significantly from those of the observed galaxy distribution, in both shape and amplitude. Thus, for any of these models to provide an acceptable representation of reality, the distribution of galaxies must be biased relative to the mass in a nontrivial, scale-dependent fashion. In the $\Omega = 1$ models, the required bias is always greater than unity, but in the $\Omega_0 = 0.3$ models, an "antibias" is required on scales smaller than $\sim 5\ h^{-1}$ Mpc. The mass correlation functions in the simulations are well fit by recently published analytic models. The velocity fields are remarkably similar in all the models, whether they are characterized as bulk flows, single-particle, or pairwise velocity dispersions. This similarity is a direct consequence of our adopted normalization and runs contrary to the common belief that the amplitude of the observed galaxy velocity fields can be used to constrain the value of Ω_0. The small-scale pairwise velocity dispersion of the dark matter is somewhat larger than recent determinations from galaxy redshift surveys, but the bulk flows predicted by our models are broadly in agreement with most available data.

Subject headings: cosmology: theory — dark matter — methods: numerical

1. INTRODUCTION

Cosmological N-body simulations play a pivotal role in the study of the formation of cosmic structure. In this methodology, initial conditions are set at some early epoch by using linear theory to calculate the statistical properties of the fluctuations. Such a calculation requires some specific mechanism for generating primordial structure, together with assumptions about the global cosmological parameters and the nature of the dominant dark matter component. N-body simulations are then used to follow the later evolution of the dark matter into the nonlinear regime where it can be compared with the large-scale structure in galaxy surveys. This general picture was developed fully in the early 1980s, building upon then novel concepts like the inflationary model of the early universe and the proposition that the dark matter is nonbaryonic. In the broadest sense, it was confirmed in the early 1990s with the discovery of fluctuations in the temperature of the microwave background radiation (Smoot et al. 1992). The plausibility of the hypothesis that the dark matter is nonbaryonic has strengthened in recent years, as the gap between the upper limit on the density of baryons from big bang nucleosynthesis considerations (e.g., Tytler, Fan, & Burles 1996) and the lower limit on the total mass density from dynamical studies (e.g., Carlberg, Yee, & Ellingson 1997) has become more firmly established.

Cosmological N-body simulations were first employed to study the large-scale evolution of dark matter on mildly nonlinear scales, a regime that can be accurately calculated using relatively few particles. Highlights of these early simulations include the demonstration of the general principles of nonlinear gravitational clustering (Gott, Turner, & Aarseth 1979); evidence that scale-free initial conditions evolve in a self-similar way (Efstathiou & Eastwood 1981; Efstathiou et al. 1985), while truncated power spectra develop large-scale pancakes and filaments (Klypin & Shandarin 1983; Centrella & Melott 1983; Frenk, White, & Davis 1983); and the rejection of the proposal that the dark matter consists of light massive neutrinos (White, Frenk, & Davis 1983; White, Davis, & Frenk 1983).

During the mid-1980s, N-body simulations were extensively used to explore the hypothesis, first elaborated by Peebles (1982), that the dark matter consists of cold collisionless particles. This hypothesis—the cold dark matter (CDM) cosmology—has survived the test of time and remains the basic framework for most contemporary cosmological work. The clustering evolution of dark matter in a CDM universe was first studied in detail using relatively small N-body simulations (Davis et al. 1985, hereafter DEFW; Frenk et al. 1985, 1988, 1990; White et al. 1987a, 1987b; Fry & Melott 1985). In particular, DEFW con-

[1] Department of Physics, South Road, University of Durham, Durham, United Kingdom DH1 3LE.
[2] CPES, University of Sussex, Falmer, Brighton, United Kingdom BN1 9QH.
[3] Max-Planck-Institut für Astrophysik, Garching bei München, D-85740, Germany.
[4] Department of Astronomy, University of Western Ontario, London, Ontario N6A 3K7, Canada.
[5] Royal Observatory, Blackford Hill, Edinburgh, United Kingdom EH9 3HJ.
[6] Department Physics, Nuclear Physics Building, Keble Road, Oxford, United Kingdom OX1 3RH.
[7] Department of Physics and Astronomy, University of Wales, P.O. Box 913, Cardiff, United Kingdom CF2 3YB.

cluded, on the basis of 32,768 particle simulations, that the simplest (or standard) version of the theory in which the mean cosmological density parameter $\Omega = 1$, and the galaxies share the same statistical distribution as the dark matter, was inconsistent with the low estimates of the root mean square (rms) pairwise peculiar velocities of galaxies that had been obtained at the time from the CfA redshift survey (Davis & Peebles 1983). They showed that much better agreement with the clustering data available at the time could be obtained in an $\Omega = 1$ CDM model if the galaxies were assumed to be biased tracers of the mass, as in the "high peak model" of galaxy formation (Kaiser 1984; Bardeen et al. 1986). They found that an equally successful CDM model could be obtained if galaxies traced the mass but $\Omega_0 \simeq 0.2$ and the geometry was either open or flat. Many of the results of this first generation of N-body simulations have been reviewed by Frenk (1991).

Following the general acceptance of cosmological simulations as a useful technique, the subject expanded very rapidly. To mention but a few examples in the general area of gravitational clustering, further simulations have reexamined the statistics of the large-scale distribution of cold dark matter (e.g., Park 1991; Gelb & Bertschinger 1994a, 1994b; Klypin, Primack, & Holtzman 1996; Cole et al. 1997; Zurek et al. 1994), confirming, on the whole, the results of the earlier, smaller calculations. Large simulations have been used to construct "mock" versions of real galaxy surveys (e.g., White et al. 1987b; Park et al. 1994; Moore et al. 1994) or to carry out "controlled experiments" designed to investigate specific effects such as non-Gaussian initial conditions (Weinberg & Cole 1992) or features in the power spectrum (Melott & Shandarin 1993). Some attempts have been made to address directly the issue of where galaxies form by modeling the evolution of cooling gas gravitationally coupled to the dark matter (e.g., Carlberg, Couchman, & Thomas 1990; Cen & Ostriker 1992; Katz, Hernquist, & Weinberg 1992; Evrard, Summers, & Davis 1994; Jenkins et al. 1997). The success of the N-body approach has stimulated the development of analytic approximations to describe the weakly nonlinear behavior, using, for example, second-order perturbation theory (e.g., Bernardeau 1994; Bouchet et al. 1995), as well as Lagrangian approximations to the fully nonlinear regime (Hamilton et al. 1991; Jain, Mo, & White 1995; Baugh & Gaztanaga 1996; Peacock & Dodds 1994, 1996; Padmanabhan 1996).

Steady progress has also been achieved on the observational front with the completion of ever larger galaxy surveys. The first real indication that the galaxy distribution on large scales differs from that predicted by the standard cold dark matter model was furnished by the Automatic Plate Measuring Facility (APM) survey, which provided projected positions and magnitudes for over a million galaxies. The angular correlation function of this survey has an amplitude that exceeds the theoretical predictions by a factor of about 3 on scales of 20–30 h^{-1} Mpc (Maddox et al. 1990). This result has been repeatedly confirmed in redshift surveys of *IRAS* (e.g., Efstathiou et al. 1990; Saunders et al. 1990; Tadros & Efstathiou 1995) and optical galaxies (e.g., Vogeley et al. 1992; Tadros & Efstathiou 1996; Tucker et al. 1997; Ratcliffe et al. 1997). Modern redshift surveys have also allowed better estimates of the peculiar velocity field of galaxies in the local universe. The original measurement of the pairwise velocity dispersion (which helped motivate the concept of biased galaxy formation in the first place) has been revised upward by Mo, Jing, & Börner (1993) and Sommerville, Davis, & Primack (1997), but Marzke et al. (1995) and Mo, Jing, & Börner (1996) have argued that such pairwise statistics are not robust when determined from relatively small redshift surveys. The Las Campanas redshift survey is, perhaps, the first that is large enough to give a robust estimate of these statistics (Jing, Mo, & Börner 1997). Surveys of galaxy distances are also now beginning to map the local mean flow field of galaxies out to large distances (e.g., Lynden-Bell et al. 1988; Courteau et al. 1993; Mould et al. 1993; Dekel et al. 1998; Giovanelli 1997; Saglia et al. 1997; Willick et al. 1997). Both pairwise velocity dispersions and mean flows allow an estimate of the parameter combination $\beta \equiv \Omega_0^{0.6}/b$ (where b is the biasing parameter defined in § 5); recent analyses seem to be converging on values of β around 0.5.

In this paper, we present results from a suite of very large, high-resolution N-body simulations. Our primary aim is to extend the N-body work of the 1980s and early 1990s by increasing the dynamic range of the simulations and calculating the low-order clustering statistics of the dark matter distribution to much higher accuracy than is possible with smaller calculations. Our simulations follow nearly 17 million particles, with a spatial resolution of a few tens of kiloparsecs, and thus probe the strong clustering regime while correctly including large-scale effects. Such improved theoretical predictions are a necessary counterpart to the high precision attainable with the largest galaxy data sets like the APM survey and particularly the forthcoming generation of redshift surveys, the Sloan (Gunn & Weinberg 1995) and two-degree field projects.[8] Our simulations do not address the issue of where galaxies form. They do, however, reveal in quantitative detail the kind of biases that must be imprinted during the galaxy formation process if any of the models is to provide an acceptable match to the galaxy clustering data. We examine four versions of the cold dark matter theory including, for the first time, the τCDM model. This has $\Omega = 1$ but more power on large scales than the standard version, and it offers an attractive alternative to the standard model if $\Omega = 1$. We focus on high-precision determinations of the spatial and velocity distributions and also carry out a comparison of the simulation results with the predictions of analytic clustering models.

Many of the issues we discuss in this paper have been addressed previously using large N-body simulations. Our study complements and supersedes aspects of this earlier work because our simulations are significantly larger and generally have better resolution than earlier simulations and also because we investigate four competing cosmological models in a uniform manner. Thus, for example, Gelb & Bertschinger (1994b) studied the standard $\Omega = 1$ CDM model, but most of their simulations had significantly poorer spatial resolution than ours, and the one with similar resolution had only 1% of the volume. Klypin et al. (1996) simulated a low-Ω_0 flat CDM model with a mass resolution at least 10 times poorer than ours or in volumes that were too small to properly include the effects of rare objects. These simulations missed a number of subtle, but nevertheless important, effects that are revealed by our larger simulations. Our analysis has some features in common with the recent work of Cole et al. (1997), who

[8] For more information, see http://www.ast.cam.ac.uk/ 2dFgg/ (this web page is neither refereed nor maintained by the Astrophysical Journal).

simulated a large suite of cosmologies in volumes that are typically 3 times larger than ours but have 3–6 times fewer particles and an effective mass resolution an order of magnitude less than ours. Their force resolution is also a factor of 3 times worse that ours. While Cole et al. focussed on models in which the primordial fluctuation amplitude is normalized using the inferred amplitude of the *COBE* microwave background fluctuations, our models are normalized so that they all give the observed abundance of rich galaxy clusters by the present day. Our choice of normalization is motivated and explained in § 3.

This study is part of the program of the "Virgo Consortium," an international collaboration recently constituted with the aim of carrying out large N-body and N-body/gasdynamic simulations of large-scale structure and galaxy formation, using parallel supercomputers in Germany and the United Kingdom. Some of our preliminary results are discussed in Jenkins et al. (1997), and further analysis of the present simulations may be found in Thomas et al. (1997).

The cosmological parameters of our models are described in § 2 and their numerical details in § 3. Color images illustrating the evolution of clustering in our simulations are presented in § 4. The evolution of the mass correlation functions and power spectra are discussed and compared with observations in §§ 5 and 6. We compare these clustering statistics with analytic models for the nonlinear evolution of correlation functions and power spectra in § 7. The present-day velocity fields, both bulk flows and pairwise dispersions, are discussed in § 8. Our paper concludes in § 9 with a discussion and summary (including a table) of our main results.

2. COSMOLOGICAL MODELS

We have simulated evolution in four CDM cosmologies with parameters suggested by a variety of recent observations. The shape of the CDM power spectrum is determined by the parameter, Γ (see eq. [4] below); observations of galaxy clustering, interpreted via the assumption that galaxies trace the mass, indicate a value of $\Gamma \simeq 0.2$ (Maddox et al. 1990; Maddox, Efstathiou, & Sutherland 1996; Vogeley et al. 1992). In the standard version of the theory, $\Gamma = \Omega_0 h$,[9] which corresponds, for low baryon density, to the standard assumption that only photons and three massless species of neutrinos and their antiparticles contribute to the relativistic energy density of the universe at late times. For a given Ω and h, smaller values of Γ are possible, but this requires additional physics, such as late decay of the (massive) τ-neutrino to produce an additional suprathermal background of relativistic e- and μ-neutrinos at the present day (White, Gelmini, & Silk 1995). This has the effect of delaying the onset of matter domination, leading to a decrease in the effective value of Γ.

In addition to observations of large-scale structure, a second consideration that has guided our choice of cosmological models is the growing evidence in favor of a value of Ω_0 around 0.3. The strongest argument for this is the comparison of the baryon fraction in rich clusters with the universal value required by big bang nucleosynthesis (White et al. 1993; White & Fabian 1995; Evrard 1997). The recently determined abundance of hot X-ray–emitting clusters at $z \simeq 0.3$ also indicates a similar value of Ω_0 (Henry 1997). The strength of these tests lies in the fact that they do not depend on uncertain assumptions regarding galaxy formation. Nevertheless, they remain controversial, and so, in addition to cosmologies with $\Omega_0 = 0.3$, we have also simulated models with $\Omega = 1$.

Three of our simulations have a power spectrum shape parameter, $\Gamma = 0.21$. One of these (ΛCDM) has $\Omega_0 = 0.3$ and the flat geometry required by standard models of inflation, i.e., $\lambda \equiv \Lambda/(3H^2) = 0.7$ (where Λ is the cosmological constant and H is Hubble's constant). The second model (OCDM) also has $\Omega_0 = 0.3$, but $\Lambda = 0$. In both of these models we take $h = 0.7$, which is consistent with a number of recent determinations (Kennicutt, Freedman, & Mould 1995). Our third model with $\Gamma = 0.21$ (τCDM) has $\Omega = 1$ and $h = 0.5$; this could correspond to the decaying neutrino model mentioned above. Finally, our fourth model is standard CDM (SCDM), which has $\Omega = 1$, $h = 0.5$, and $\Gamma = 0.5$. Thus, two of our models (ΛCDM and OCDM) differ only in the value of the cosmological constant, two others (ΛCDM and τCDM) have the same power spectrum and geometry but different values of Ω_0, and two more (τCDM and SCDM) differ only in the shape of the power spectrum.

Having chosen the cosmological parameters, we must now set the amplitude of the initial fluctuation spectrum. DEFW did this by requiring that the slope of the present-day two-point galaxy correlation function in the simulations should match observations. This was a rather crude method, but one of the few practical alternatives with the data available at the time. The discovery of fluctuations in the temperature of the microwave background radiation by *COBE* offered the possibility of normalizing the mass fluctuations directly by relating these to the measured temperature fluctuations on large scales. In practice, however, the large extrapolation required to predict the amplitude of fluctuations on scales relevant to galaxy clustering from the *COBE* data makes this procedure unreliable because it depends sensitively on an uncertain assumption about the slope of the primordial power spectrum. A further source of uncertainty is the unknown contribution to the *COBE* signal from tensor (rather than scalar) modes. In spite of these uncertainties, it is remarkable that the normalization inferred from the simplest possible interpretation of the *COBE* data is within about a factor of 2 of the normalization inferred for standard CDM by DEFW from galaxy clustering considerations.

A more satisfactory procedure for fixing the amplitude of the initial mass fluctuations is to require that the models match the observed abundance of galaxy clusters. The distribution of cluster abundance, characterized by mass, X-ray temperature, or some other property, declines exponentially and so is very sensitive to the normalization of the power spectrum (Frenk et al. 1990). Using the observed cluster abundance to normalize the power spectrum has several advantages. First, it is based on data that are well matched to the scales of interest; second, it gives the value of σ_8 (the linearly extrapolated rms of the density field in spheres of radius $8\ h^{-1}$ Mpc) with only a weak dependence on the shape of the power spectrum if $\Omega < 1$ and no dependence at all if $\Omega = 1$ (White, Efstathiou, & Frenk 1993); and third, it does not require a particularly accurate estimate of the abundance of clusters because of the strong sensitivity of abundance on σ_8. The disadvantage of this method is that it is sensitive to systematic biases arising from inaccurate

[9] Here and below we denote Hubble's constant, H_0, by $h = H_0/100$ km s^{-1} Mpc^{-1}.

determinations of the particular property used to characterize the abundance. However, the consistency of the estimates of σ_8 when the abundance of clusters is characterized by total mass (Henry & Arnaud 1991), by mass within the Abell radius (White et al. 1993), or by the X-ray temperature of the intracluster medium (Eke, Cole, & Frenk 1996; Viana & Liddle 1996) suggests that systematic effects are likely to be small.

We adopt the values of σ_8 recommended by Eke et al. (1996) from their analysis of the local cluster X-ray temperature function. This requires

$$\sigma_8 = (0.52 \pm 0.04)\Omega_0^{-0.52+0.13\Omega_0} \quad \text{(flat models)} \qquad (1)$$

or

$$\sigma_8 = (0.52 \pm 0.04)\Omega_0^{-0.46+0.1\Omega_0} \quad \text{(open models)} . \qquad (2)$$

These values of σ_8 are consistent with those obtained from the slightly different analyses carried out by White et al. (1993), Viana & Liddle (1996), and Henry (1997).

The resulting values of σ_8 for our simulations are listed in Table 1. For reference, these values may be compared to those required by the *COBE* data under the simplest set of assumptions, namely that the primordial power spectrum is a power law with exponent $n = 1$ (the Harrison-Zeldovich spectrum) and that there is no contribution at all from tensor modes. For our chosen cosmologies, the 4 year *COBE*-Differential Microwave Radiometer (DMR) data imply values of σ_8 of 1.21, 0.45, 1.07, and 0.52 (Górski et al. 1995; Ratra et al. 1997) for SCDM, τCDM, ΛCDM, and OCDM, respectively. Thus, our τCDM and ΛCDM models are roughly consistent with the conventional *COBE* normalization, but our adopted normalizations for the SCDM and OCDM models are $\sim$40% lower and $\sim$60% higher, respectively, than the *COBE* values. These numbers are consistent with those obtained by Cole et al. (1997) from their grid of large *COBE*-normalized cosmological *N*-body simulations with different parameter values. As may be seen from their Figure 4, there is only a small region of parameter space in which the conventional *COBE*-normalized CDM models produce the correct abundance of clusters. Flat models require $0.25 \leq \Omega_0 \leq 0.4$, while open models require $0.4 \leq \Omega_0 \leq 0.5$.

To summarize, we have chosen to simulate four cosmological models that are of interest for a variety of reasons. Our three flat models are consistent with standard inflationary theory, and our open model can be motivated by the more exotic "open bubble" version of this theory (Garcia-Bellido & Linde 1997). By construction, all of our models approximately reproduce the observed abundance of rich galaxy clusters. The ΛCDM model has a value of Ω_0 in line with recent observational trends and a value of Γ that is close to that inferred from galaxy clustering. It has the additional advantages that its normalization agrees approximately with the conventional *COBE* normalization and, for our adopted value of H_0, it has an age that is comfortably in accord with traditional estimates of the ages of globular clusters (Renzini et al. 1996; but see Jimenez et al. 1996). The OCDM model shares some of these attractive features but allows us also to investigate the effects of the cosmological constant on the dynamics of gravitational clustering. Its normalization is higher than required to match the conventional *COBE* value, but this could be rectified by a modest increase in Ω_0 to about 0.4–0.5. The τCDM model is as well motivated by galaxy clustering data, as are the low-Ω_0 models, and has the advantage that it allows us to investigate the dynamical effects of changing Ω_0 while keeping the shape of the initial power spectrum fixed. Finally, the traditional SCDM model is an instructive counterpart to its τCDM variant.

3. THE SIMULATIONS

Our simulations were carried out using a parallel, adaptive particle-particle/particle-mesh code developed by the Virgo Consortium (Pearce et al. 1995; Pearce & Couchman 1997). This is identical in operation to the publicly released serial version of "Hydra" (Couchman, Pearce, & Thomas 1996; see Couchman, Thomas, & Pearce 1995 for a detailed description). The simulations presented in this paper are the first carried out by the Virgo Consortium and were executed on either 128 or 256 processors of the Cray T3Ds at the Edinburgh Parallel Computing Centre and the Rechenzentrum, Garching.

The force calculation proceeds through several stages. Long-range gravitational forces are computed in parallel by smoothing the mass distribution onto a mesh, typically containing 512^3 cells, which is then fast Fourier transformed and convolved with the appropriate Green's function. After an inverse fast Fourier transform, the forces are interpolated from the mesh back to the particle positions. In weakly clustered regions, short-range (particle-particle) forces are also computed in parallel using the entire processor set. Hydra recursively places additional higher resolution meshes, or *refinements*, around clustered regions. Large refinements containing over $\simeq 10^5$ particles are executed in parallel by all processors while smaller refinements, which fit within the memory of a single processor, are most efficiently executed using a task farm approach. The parallel version of Hydra employed in this paper is implemented in CRAFT, a directive based parallel Fortran compiler developed for the Cray T3D supercomputer (Cray Research Inc.

TABLE 1

COSMOLOGICAL AND NUMERICAL PARAMETERS OF RUNS

Run	Ω_0	Λ	h	Γ	σ_8	$(h^{-1}$ Mpc)	Number of Particles	m_p $(h^{-1} M_\odot)$	l_{soft} $(h^{-1}$ Kpc)
SCDM1	1.0	0.0	0.5	0.50	0.51	239.5	256^3	2.27×10^{11}	36
τCDM1a	1.0	0.0	0.5	0.21	0.51	239.5	256^3	2.27×10^{11}	36
τCDM1ab.....	1.0	0.0	0.5	0.21	0.51	239.5	256^3	2.27×10^{11}	36
ΛCDM1.....	0.3	0.7	0.7	0.21	0.90	239.5	256^3	6.86×10^{10}	25
OCDM1	0.3	0.0	0.7	0.21	0.85	239.5	256^3	6.86×10^{10}	30
SCDM2	1.0	0.0	0.5	0.50	0.51	84.5	256^3	1.00×10^{10}	36
τCDM2	1.0	0.0	0.5	0.21	0.51	84.5	256^3	1.00×10^{10}	36
ΛCDM2.....	0.3	0.7	0.7	0.21	0.90	141.3	256^3	1.40×10^{10}	30
OCDM2	0.3	0.0	0.7	0.21	0.85	141.3	256^3	1.40×10^{10}	30

1900). We have checked that the introduction of mesh refinements in high-density regions does not introduce inaccuracies in the computation by redoing our standard τCDM simulation using a parallel P^{3}M code (without refinements). The two-point correlation functions in these two simulations differed by less than 0.5% over the range 0.1–5 h^{-1} Mpc.

3.1. *Simulation Details*

Initial conditions were laid down by imposing perturbations on an initially uniform state represented by a "glass" distribution of particles generated by the method of White (1996). Using the algorithm described by Efstathiou et al. (1985), which is based on the Zeldovich (1970) approximation, a Gaussian random field is set up by perturbing the positions of the particles and assigning them velocities according to growing mode linear theory solutions. Individual modes are assigned random phases, and the power for each mode is selected at random from an exponential distribution with mean power corresponding to the desired power spectrum, $\Delta^2(k)$.

Following Peebles' (1980) convention, we define the dimensionless power spectrum, $\Delta^2(k)$, as the power per logarithmic interval in spatial frequency, k:

$$\Delta^2(k) \equiv \frac{V}{(2\pi)^3} 4\pi k^3 |2\delta_k|^2 , \quad (3)$$

where $|\delta_k|^2$ is the power density, and V is the volume. If the primordial power spectrum is of the form $|\delta_k|^2 \propto k^n$, then the linear power spectrum at a later epoch is given by $\Delta^2(k) = k^{n+3}T^2(k, t)$, where $T(k, t)$ is the transfer function. The standard inflationary model of the early universe predicts that $n \simeq 1$ (Guth & Pi 1981), and we shall take $n = 1$. For a cold dark matter model, the transfer function depends on the values of h and the mean baryon density, Ω_b. We use the approximation to the linear CDM power spectrum given by Bond & Efstathiou (1984),

$$\Delta^2(k) = \frac{Ak^4}{\{1 + [aq + (bq)^{3/2} + (cq)^2]^\nu\}^{2/\nu}} , \quad (4)$$

where $q = k/\Gamma$, $a = 6.4\ h^{-1}$ Mpc, $b = 3\ h^{-1}$ Mpc, $c = 1.7\ h^{-1}$ Mpc, and $\nu = 1.13$. The normalization constant, A, is chosen by fixing the value of σ_8 as discussed in § 2.

For our models, the analytic approximation of equation (4) provides a good approximation to the accurate numerical power spectrum calculated by Seljak & Zaldarriaga (1996) using their code CMBFAST.[10] For example, setting $h = 0.7$ and $\Omega_b = 0.026$ in our ΛCDM and OCDM and normalizing to the same value of σ_8, we find that the maximum difference at small scales between the fit of equation (4) and the output of CMBFAST is 13% in power or 6% in amplitude. These numbers are smaller for a lower value of Ω_b or a small increase in h. These differences are comparable to those induced by plausible changes in Ω_b or h. (For example, for a ΛCDM model, the ratio of the σ_8-normalized CMBFAST power spectra for $\Omega_b = 0.01$ and $\Omega_b = 0.03$, respectively, is 1.08 at the Nyquist frequency of our simulation volumes [$k = 3.36\ h$ Mpc^{-1}] and 0.85 at the fundamental frequency [$k = 0.0262\ h$ Mpc^{-1}]; if Ω_b is kept fixed but h is allowed to vary between 0.67 and 0.73, these ratios become 1.08 and 0.9, respectively.) Similarly, we set up our τCDM model simply by changing the value of Γ in equation (4). This gives a satisfactory fit provided that the length-scale introduced in the power spectrum by the decay of the τ-neutrino is smaller than Nyquist frequency of the simulation volume. This requires the mass of the decaying particle to be in excess of about 10 keV (Bond & Efstathiou 1991). Thus, over the range of wavenumbers relevant to our simulations, equation (4) gives a good, but not perfect, approximation to the true τCDM power spectrum for a broad one-dimensional subset of the two-dimensional mass-lifetime space for the τ-neutrino (see White et al. 1995). Again, these differences are small compared to those induced by changes, similar to those above, in Ω_b and h. Finally, as discussed above, the normalization of the power spectrum from the cluster abundance is uncertain by at least 15% (1 σ) (Eke et al. 1996). These various uncertainties limit the accuracy with which the dark matter distribution can be calculated at the present time.

For each cosmological model, we analyze two simulations of regions of differing size. To facilitate intercomparison, we employed the same random number sequence to generate initial conditions for all of these simulations. To test for finite volume effects, however, we carried out an additional simulation of the τCDM model, this time using a different realization of the initial conditions. In the first set of simulations (which includes the extra τCDM model), we adopted a box length of $L = 239.5\ h^{-1}$ Mpc. The gravitational softening length was initially set to 0.3 times the grid spacing and was kept constant in comoving coordinates until it reached the value given in Table 1, at $z \simeq 3$. Thereafter, it was kept constant in physical units. (The functional form of the gravitational softening used is that given by Efstathiou & Eastwood 1981; the values we quote correspond to the softening scale of a Plummer potential, which matches the actual force law asymptotically at both large and small scales. The actual force is 53.6% of the full $1/r^2$ force at one softening length and more than 99% at two softening lengths.) In the second set of simulations, the particle mass in solar masses (rather than the volume) was kept constant in all four models, and the gravitational softening was taken to be either 30 or 36 h^{-1} kpc in physical units (after initially being kept fixed in comoving coordinates as before). The mass resolution in these simulations is a factor of 3–20 better than in the first set. The large box simulations are large enough to give unbiased results and relatively small sampling fluctuations for all of the statistics we study, with the exception of large-scale bulk flows. For example, on scales less than 5 h^{-1} Mpc, the typical differences in the correlation function and pairwise velocities of the two τCDM realizations are only about 2%. We use the large box simulations for most of our analysis of large-scale clustering and velocities (§§ 5, 6, 8). The smaller volume simulations, on the other hand, resolve structures down to smaller mass scales. We use these to test the effects of numerical resolution and for a comparison with analytic models in § 7, where special emphasis is given to the strong clustering regime. All of our simulations have 16.7 million particles. The number of time steps varied between 613 and 1588. The SCDM and τCDM simulations were started at $z = 50$; the OCDM were started at $z = 119$, and the ΛCDM at $z = 30$. The parameters of our simulations are listed in Table 1.

[10] Publicly available at http://arcturus.mit.edu:80/ ~ matiasz/CMBFAST /cmbfast.html. This website contains information that has not been refereed, neither is it maintained by the Astrophysical Journal.

4. SLICES THROUGH THE SIMULATIONS

Figures 1–3 (Plates 1–3) show slices through the dark matter distribution in our four models at three different redshifts: $z = 0$, 1, and 3. The slices are 239.5 h^{-1} Mpc on a side and have thickness 1/10 of the side length. The projected mass distribution in these slices was smoothed adaptively onto a fine grid employing a variable kernel technique similar to that used to estimate gas densities in smoothed particle hydrodynamics.

At $z = 0$, the general appearance of all of the models is similar because, by construction, the phases of the initial fluctuations are the same. The now-familiar pattern of interconnected large-scale filaments and voids is clearly apparent. However, at the high resolution of these simulations, individual galactic dark halos are also visible as dense clumps of a few particles. On larger scales, the higher fluctuation amplitude in the ΛCDM and OCDM models is manifest in sharper filaments and larger voids compared to the SCDM and τCDM models. Because of their higher normalization, the low-Ω_0 models also have more small-scale power than SCDM and τCDM, and this results in tighter virialized clumps. The linearly evolved power spectra of ΛCDM and OCDM are almost identical, and so the primary differences between them reflect their late-time dynamics, dominated by the cosmological constant in one case and by curvature in the other. In OCDM, structures of a given mass collapse earlier and so are more compact than in ΛCDM. The fine structure in SCDM and τCDM is similar, but since the relative amounts of power in these models cross over at intermediate scales, clumps are slightly fuzzier in the τCDM case.

The large-scale differences among the models are much more apparent at $z = 1$. There is substantially more evolution for $\Omega = 1$ than for low-Ω_0; in the former case, the linear growth factor is 0.50 of the present value, whereas in ΛCDM and OCDM, it is 0.61 and 0.68, respectively. Thus, OCDM has the most developed large-scale structure at $z = 1$, while ΛCDM is intermediate between this and the two $\Omega = 1$ models. By $z = 1$, the OCDM model has already become curvature dominated ($\Omega = 0.46$), but the cosmological constant is still relatively unimportant in the ΛCDM model ($\Omega = 0.77$).

At the earliest epoch shown, $z = 3$, the differences between the models are even more striking. The linear growth factor for SCDM and τCDM is 0.25, while for ΛCDM it is 0.32 and for OCDM 0.41 of its present value. The SCDM model is very smooth, with only little fine structure. The τCDM model has some embryonic large-scale structure, but it is even more featureless than SCDM on the finest scales. By contrast, structure in the low-Ω_0 models, particularly OCDM, is already well developed by $z = 3$.

5. THE TWO-POINT CORRELATION FUNCTIONS

In this section we discuss the redshift evolution of the mass two-point correlation function, $\xi(r)$, and compare the results at $z = 0$ with estimates for the observed galaxy distribution.

For each volume, we have a single simulation from which to estimate $\xi(r)$. Since this volume is assumed to be periodic, contributions to the correlation function from long-wavelength modes are poorly sampled. In principle, it is possible to add a systematic correction, based on the linear theory growth of long wavelength modes (see the Appendix for a derivation):

$$\Delta\xi(\boldsymbol{r}) = \sum_{\boldsymbol{n}\neq(0,0,0)}^{\infty} - \xi_{\rm lin}(|\boldsymbol{r} + L\boldsymbol{n}|)\,, \tag{5}$$

where L is the simulation box length, and $\xi_{\rm lin}$ is the linear theory correlation function given in terms of the linearly evolved power spectrum, $\Delta^2_{\rm lin}$, by

$$\xi_{\rm lin}(r) = \int_0^\infty \Delta^2_{\rm lin}\left(\frac{\sin kr}{kr}\right)\frac{dk}{k}\,. \tag{6}$$

This expression gives a correction that is negligible for most of our simulation volumes. For example, for τCDM2, our simulation with the smallest box size ($L = 84.5$ h^{-1} Mpc) and substantial large-scale power ($\Gamma = 0.21$), the correction is only 0.01 at small separations. The expression in equation (5) is approximately a factor of 3 smaller for the 84.5 h^{-1} Mpc volume than the heuristic correction, $\int_0^{2\pi/L} \Delta^2(\sin kr/kr)dk/k$, used by Klypin et al. (1996). In any case, for a single simulation, there is also a random error associated with the fact that the power originally assigned to each mode is drawn from a distribution. This introduces a random scatter in the correlation function which is comparable to the correction in equation (5). The most direct way of assessing the importance of this effect in our simulations is by comparing two or more realizations of the same model. For the case of τCDM, we have carried out a second simulation with identical parameters to the first one but using a different random number seed to set up initial conditions. The difference between the correlation functions of these two simulations is less than 2% on all scales below 5 h^{-1} Mpc, comparable to the thickness of the line used to plot them in Figure 5 below.

On small scales, the amplitude of the two-point correlation function is suppressed by resolution effects due to the use of softened gravity and finite mass resolution. To test the first of these effects, we performed a series of three simulations of the τCDM model with 128^3 particles, identical initial conditions, the same mass resolution as the τCDM1a simulation, and three different values of the gravitational softening length. The resulting two-point correlation functions are shown in Figure 4. The effects on the correlation function at twice the softening length are very small. Similarly, mass resolution effects in our simulations are small, as we discuss later in this section and in § 7.

Figure 5 shows the mass two-point correlation functions in our four cosmological models at four different epochs. These data were computed using the simulations SCDM1, τCDM1a, ΛCDM1, and OCDM1. As the clustering grows, the amplitude of the correlation function increases in a nonlinear fashion. The overall shape of $\xi(r)$ is similar in all the models. In all cases, $d^2\xi/dr^2 < 0$ on scales below $r \sim 500$ h^{-1} kpc, and there is an inflection point on scales of a few megaparsecs. The flattening off of $\xi(r)$ at small pair separations is unlikely to be a numerical artifact. It occurs on scales that are several times larger than the gravitational softening length and are well resolved. That this change in slope is not due to mass resolution effects (associated, for example, with the limited dynamic range of the initial conditions) is demonstrated by the excellent agreement between the small-scale behavior of the correlation functions plotted in Figure 5 and the correlation functions of our smaller volume simulations that have 3–20 times better mass resolution (see Fig. 8 below; see also Little, Weinberg,

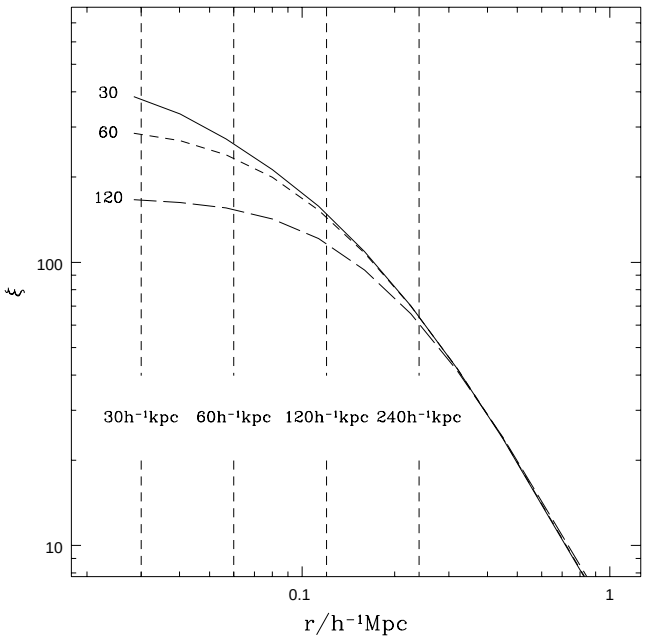

FIG. 4.—Effect of the gravitational softening length on the two-point correlation function. The curves show results for three 128^3 particle simulations of the τCDM model with identical initial conditions but with gravitational softening lengths of 30, 60, and 120 h^{-1} kpc, respectively. Beyond twice the softening length, the effect on the correlation function is small.

& Park 1991 for a discussion of why neglecting the power below the Nyquist frequency of the initial conditions has little effect on nonlinear evolution). Rather, the flattening of $\xi(r)$ at small pair separations seems to be due to the transition into the "stable clustering" regime. We return to this point in § 7, where we compare the correlation functions in the simulations with analytic models for nonlinear evolution.

The mass correlation functions at $z = 0$ (*thick solid lines*) may be compared with the observed galaxy correlation function. The largest data set available for this comparison is the APM galaxy survey of over 10^6 galaxies, for which Baugh (1996) has derived the two-point correlation function, $\xi_g(r)$, by inverting the measured angular correlation function, $w(\theta)$. The advantage of this procedure is that it gives a very accurate estimate of the correlation function in real space, but the disadvantage is that it requires assumptions for the redshift distribution of the survey galaxies and for the evolution of $\xi_g(r)$ in the (relatively small) redshift range sampled by the survey. The solid line with error bars in Figure 5 assumes that clustering on all scales is fixed in comoving coordinates, while the dotted line assumes that clustering evolves in proportion to the scale factor. Changes in the assumed redshift distribution produce a systematic scaling of the entire correlation function. On scales $\gtrsim 20$–30 h^{-1} Mpc, the statistical error bars may underestimate the true uncertainty in $\xi_g(r)$, since residual systematic errors in the APM survey on these scales cannot be ruled out (Maddox et al. 1996).

None of the model mass correlation functions match the shape of the observed galaxy correlation function. For the galaxies, $\xi_g(r)$ is remarkably close to a power law over 4 orders of magnitude in amplitude above $\xi_g = 1$; at larger pair separations, it has a broad shoulder feature. By contrast, the slope of the mass correlation functions in the models varies systematically, so that none of the theoretical curves is adequately fit by a single power law over a substantial range of scales. We have checked (C. M. Baugh 1997, private communication) that the inversion procedure used to derive the APM $\xi_g(r)$ from the measured $w(\theta)$ does not artificially smooth over features that may be present in the intrinsic clustering pattern. We have also checked that features present in the model $\xi(r)$ are still identifiable in the corresponding $w(\theta)$ derived with the same assumptions used in the APM analysis. The differences in shape and amplitude between the theoretical and observed correlation functions may be conveniently expressed as a "bias function." We define the bias as the square root of the ratio of the observed galaxy to the theoretical mass correlation functions at $z = 0$, $b(r) \equiv [\xi_g(r)/\xi(r)]^{1/2}$ and plot this function at the bottom of each panel in Figure 5. At each pair separation, $b(r)$ gives the factor by which the galaxy distribution should be biased in order for the particular model to match observations. For all the models considered here, the required bias varies with pair separation.

The standard CDM model, illustrated in the top left panel, shows the well-known shortfall in clustering amplitude relative to the galaxy distribution on scales greater than 8 h^{-1} Mpc. The required bias is close to unity on scales of 0.1–1 h^{-1} Mpc but then rises rapidly with increasing scale. The choice of $\Gamma = 0.21$ for the other models leads to mass correlation functions with shapes that are closer to that of the galaxies on large scales. For these models, the slope of the bias function is relatively modest on scales $\gtrsim 10$ h^{-1} Mpc. The large-scale behavior of $b(r)$, however, may be affected by possible systematic errors in the APM $w(\theta)$ at large pair separations and by finite box effects in the simulations. The τCDM model, which has the smallest amount of small-scale power, requires a significant positive bias everywhere, $b \simeq 1.5$, and this is approximately independent of scale from ~ 0.2–10 h^{-1} Mpc. At smaller pair separations, the bias increases rapidly. As discussed in the next section, the power spectrum, which is less affected by finite box effects than the correlation function, indicates that a constant bias for the τCDM model is consistent with the APM data even on scales larger than 10 h^{-1} Mpc. Thus, uniquely among the models we are considering, the shape of the correlation function and power spectrum in the τCDM model are quite similar to the observations on scales $\gtrsim 0.2$ h^{-1} Mpc.

In the ΛCDM and OCDM models, the amplitude of the dark matter, $\xi(r)$, is close to unity at $r = 5$ h^{-1} Mpc, the pair separation at which $\xi_g(r)$ is also close to unity. However, at small pair separations, the mass correlation function has a much steeper slope than the galaxy correlation function, and, as result, $\xi(r)$ rises well above the galaxy data. Thus, our low-density models require an "antibias," i.e., a bias less than unity, on scales $\simeq 0.1$–4 h^{-1} Mpc. A similar conclusion was reached by Klypin et al. (1996) from a lower resolution N-body simulation of a similar ΛCDM model. As pointed out by Cole et al. (1997), the requirement that galaxies be less clustered than the mass must be regarded as a negative feature of these models. Even if a plausible physical process could be identified that would segregate galaxies and mass in this manner, dynamical determinations of Ω_0 from cluster mass-to-light ratios tend to give values of $\Omega_0 \simeq 0.2$ if the galaxies are assumed to trace the mass (e.g., Carlberg et al. 1997). If, instead, the galaxy distribution were actually antibiased, this argument would result in an overestimate of

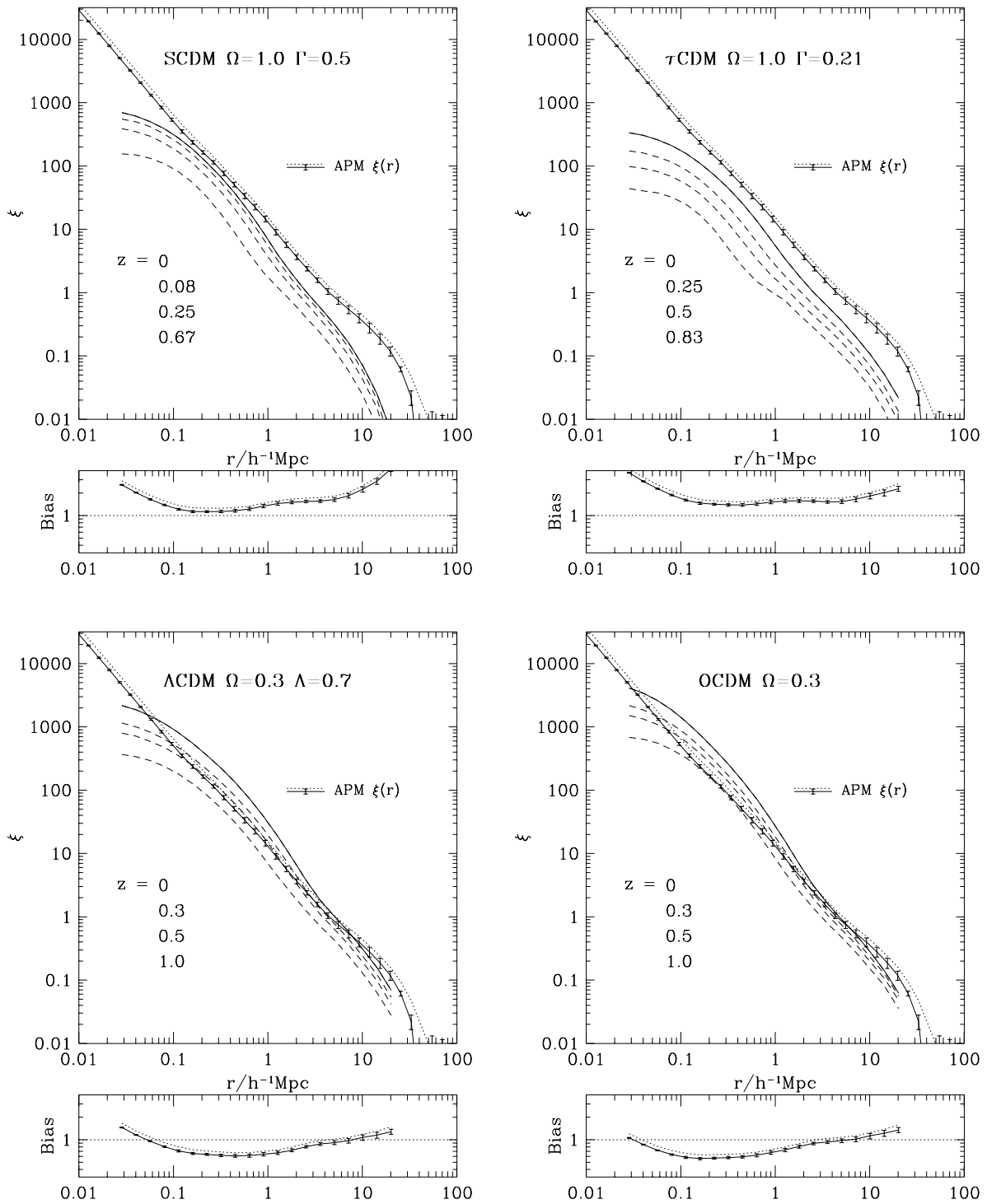

FIG. 5.—Evolution of the mass correlation function, $\xi(r)$. The top panels show the two-point correlation function in our four models at the redshifts given in the legend, with results at $z = 0$ plotted as a heavy solid line. The galaxy correlation function for the APM galaxy survey, determined by Baugh (1996), is shown as a solid line with error bars and as a dotted line. The former corresponds to the assumption that clustering is fixed in comoving coordinates and the latter to the assumption that clustering evolves in proportion to the scale factor. The small panels below each $\xi(r)$ plot show the square root of the ratio of the observed galaxy to the theoretical mass correlation functions at $z = 0$. This ratio is the bias in the galaxy distribution that would be required for the particular model to match the observations.

the true value of Ω_0. Models with Ω_0 smaller than our adopted value of 0.3 require even larger values of σ_8, and therefore even larger antibias, in order to match the observed abundance of galaxy clusters. In our $\Omega = 1$ models, the required bias always remains above unity and is, in fact, quite close to unity over a large range in scales. This is an attractive feature of these models that may help reconcile them with virial analyses of galaxy clusters (Frenk et al. 1996), and results, in part, from the relatively low normalization required to match the cluster abundance. However, the bias we infer is only about 60% of the value required by Frenk et al. (1990) to obtain acceptable cluster

mass-to-light ratios in an $\Omega = 1$ CDM cosmology with "high peak" biasing.

It seems almost inevitable that the process of galaxy formation and subsequent dynamical evolution will bias the galaxy distribution relative to the mass in a complicated way. Indeed, a variety of biasing mechanisms have been discussed in the past. These are essentially of two types. In the first, galaxy formation is assumed to be modulated, for example, by the local value of the density smoothed on cluster scales, as in the high peak bias model of galaxy formation (Bardeen et al. 1986; DEFW), or by the effects of a previous generation of protogalaxies (e.g., Dekel & Rees 1987). Such local processes tend to imprint features on the galaxy correlation function on small and intermediate scales, but Coles (1993) and Weinberg (1995) have argued that they do not appreciably distort the shape of the mass correlation function on large scales. This, however, may be achieved by some form of nonlocal bias as in the "cooperative galaxy formation" scheme proposed by Bower et al. (1993; see also Babul & White 1991). In this case, a match to the APM $w(\theta)$ on large scales is possible with a suitable choice of model parameters. The second type of biasing mechanism is of dynamical origin. An example is the "natural bias" found in the CDM simulations of White et al. (1987b), who showed that the dependence of fluctuation growth rate on mean density naturally biases the distribution of massive dark halos toward high-density regions (see also Cen & Ostriker 1992). Another example is dynamical friction which, as Richstone, Loeb, & Turner (1992) and Frenk et al. (1996) among others have shown, can segregate galaxies from mass in rich clusters. Dynamical biases of this type tend to enhance the pair count at small separations, flattening the bias function on scales of a few hundred kiloparsecs. Mergers, on the other hand, have the opposite effect and may even give rise to an antibias of the kind required in our low-Ω_0 models (cf. Jenkins et al. 1997). Thus, it seems likely that the correlation function of the *galaxies* that would form in our models will differ from the correlation function of the mass. Nevertheless, the fine tuning required to end up with an almost featureless power-law correlation function over at least 2 orders of magnitude in scale seems a considerable challenge for this general class of models.

6. THE POWER SPECTRA

For an isotropic distribution in k-space, the power spectrum is related to the correlation function by

$$\xi(r) = \int_0^\infty \Delta^2(k) \left(\frac{\sin kr}{kr} \right) \frac{dk}{k} . \tag{7}$$

To measure the power spectrum of our simulations over a wide range of scales, we use a technique that is efficient both in terms of computational expense and memory. To evaluate the power spectrum on the smallest scales, we divide the computational volume into m^3 equal cubical cells and superpose the particle distributions of all m^3 cells. The Fourier transform of this density distribution, which is now periodic on a scale L/m, recovers exactly the power present in the full simulation volume in modes that are periodic on the scale L/m. These modes form a regular grid of spacing $2m\pi/L$ in $\boldsymbol{k}$-space. The estimate of $\Delta^2(r)$ is obtained by averaging the power of large numbers of modes in spherical shells. Provided these modes have, on average, representative power, this gives an unbiased estimate of the power spectrum of the simulation. In principle, the power of all the modes in the full simulation can be obtained by applying a complex weighting, $\exp(2\pi i \boldsymbol{n} \cdot \boldsymbol{r}/L)$, to a particle at position $\boldsymbol{r}$ during the charge assignment prior to taking the discrete fast Fourier transform. This charge assignment creates a uniform translation in $\boldsymbol{k}$-space by $2\pi\boldsymbol{n}/L$. With a suitable choice of $\boldsymbol{n}$, one can recover a different set of modes from the original simulation, always with a spacing of $2m\pi/L$ in $\boldsymbol{k}$-space. Applying this method m^3 times allows the recovery of all modes present in the simulation, although there is no longer any gain in CPU time over a single large fast Fourier transform. Because of the sparse sampling of $\boldsymbol{k}$-space, the estimate of the power on the scale L/m has a large variance. However, by using a 64^3 mesh and evaluating the Fourier transform for several values of m, one can evaluate the power spectrum on any scale with adequate sampling and avoid this problem except for $m = 1$.

The assumption that these sparsely sampled modes carry representative power is true by construction in the initial conditions. The violation of this assumption as a result of nonlinear evolution is very unlikely because it would require a detailed large-scale ordering to develop over the simulation. This may, however, come about artificially; for example, the MAPS procedure of Tormen & Bertschinger (1996; see also Cole 1997), which is designed to extend the dynamic range of an N-body cosmological simulation, requires periodically replicating a simulation and then modifying the large-scale modes so as to effectively add large-scale power not present in the original simulation. In this case, the large-scale order that arises by the replication introduces significant fine-scale structure in k-space (Cole 1997), and one should be wary when applying this method.

Figure 6 shows the time evolution of the power spectrum for the same four simulations ($L = 239.5\ h^{-1}$ Mpc) illustrated in Figure 5. As before, two graphs are shown for each model. The larger one gives the time evolution of the power spectrum, plotted at four different epochs. The $z = 0$ results may be compared with the three-dimensional power spectrum of the APM galaxy survey (Baugh & Efstathiou 1993). As for the correlation function, two versions of the APM power spectrum are plotted, one assuming that the clustering pattern remains fixed in comoving coordinates (*solid curve with error bars*) and the other assuming that it evolves in proportion to the scale factor (*dotted curve*). For wavenumbers $k < 0.086\ h$/Mpc, we have plotted the linear theory power spectrum rather than the simulation results since the sparse sampling of the modes with wavelength comparable to the simulation box size gives rise to spurious fluctuations. The linear extrapolation can be seen to join smoothly onto the actual power spectrum on these scales. The smaller panels show the square root of the ratio of the APM galaxy power spectrum to that of the dark matter in the simulation at $z = 0$. As before, this is the scale-dependent bias required in the galaxy distribution for a particular model to be a good match to the APM data.

Comparison of the APM data with the power spectrum of the dark matter in the different cosmological models brings out essentially the same features as the corresponding comparison with the correlation function. In the SCDM model, the dark matter power spectrum falls below that of the galaxies at small wavenumbers, requiring a bias function that increases rapidly at small k. The shape of the power spectrum in the low-Ω_0 models is similar to that of

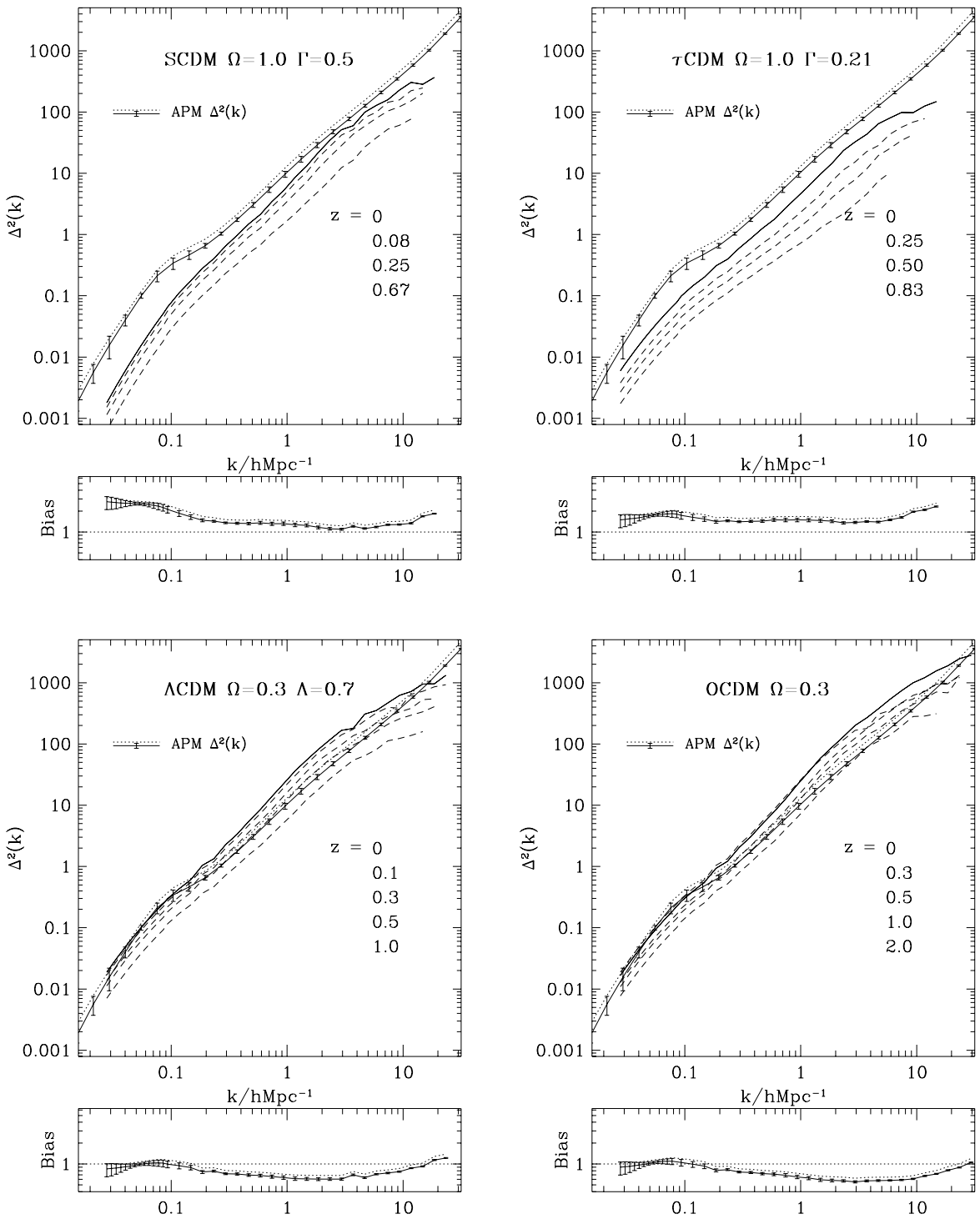

FIG. 6.—Evolution of the power spectrum of the dark matter in the simulations. The large panels show the power spectrum evaluated at the redshifts given in the figure legend, with results at $z = 0$ shown as a solid line. The solid line with error bars and the dotted line are estimates of the power spectrum of the APM galaxy survey obtained assuming, respectively, that clustering is fixed in comoving coordinates or that it grows with the scale factor (Baugh & Efstathiou 1991). The small panels show the square root of the ratio of the APM galaxy power spectrum to the present-day dark matter spectrum. This ratio is the bias in the galaxy distribution required for the model to match the APM data. For $k < 0.086\ h\ \mathrm{Mpc}^{-1}$, the linear theory power spectrum has been plotted, rather than the actual spectrum, which is noisy due to the small number of modes that contribute to each bin.

the APM galaxies only for $k < 0.1\ h$/Mpc; at larger k the dark matter distribution has more power than the galaxy distribution, requiring a bias less than unity. Only the τCDM model has a dark matter power spectrum whose shape matches that of the galaxy data over a wide range of scales. The required bias in this case is approximately constant for $0.02 \lesssim k/h\ \mathrm{Mpc}^{-1} \lesssim 10$.

7. COMPARISON WITH ANALYTIC PREDICTIONS

We now compare the results of our simulations with a parameterized fitting formula that Peacock & Dodds (1996) use to predict the power spectrum of the nonlinear mass density field which develops through gravitational amplification of any given Gaussian field of linear density fluctua-

tions. We consider both the power spectrum and the correlation function. We first summarize the theory and then compare it with the simulation results discussed in §§ 5 and 6.

7.1. *Method*

Hamilton et al. (1991) suggested a formalism for computing the nonlinear growth of the two-point correlation function. Peacock & Dodds (1994) adapted this method to the computation of nonlinear power spectra and extended it to cosmologies with $\Omega_0 \neq 1$. Baugh & Gaztanaga (1996) applied it to the power spectrum of the APM galaxy survey. The original formalism of Hamilton et al. (1991) was independent of the shape of the power spectrum, but Jain et al. (1995) showed that this is not correct. Peacock & Dodds (1996) give an improved version of the Peacock & Dodds (1994) method that takes this into account and allows the nonlinear spectrum produced by evolution from any smoothly varying linear spectrum to be calculated. Smith et al. (1997) have tested the new procedure with a large number of N-body simulations. The method may be summarized as follows.

The nonlinear spectrum is a function of the linear spectrum at a smaller linear wavenumber:

$$\Delta^2_{\rm NL}(k_{\rm NL}) = f_{\rm NL}[\Delta^2_L(k_L)] \,, \tag{8}$$

$$k_L = [1 + \Delta^2_{\rm NL}(k_{\rm NL})]^{-1/3} k_{\rm NL} \,. \tag{9}$$

The following fitting formula for the nonlinear function, $f_{\rm NL}$, was proposed by Peacock & Dodds (1996):

$$f_{\rm NL}(x) = x\left(\frac{1 + B\beta x + [Ax]^{\alpha\beta}}{1 + \{[Ax]^{\alpha} g^3(\Omega_0)/[Vx^{1/2}]\}^{\beta}}\right)^{1/\beta} . \tag{10}$$

In this expression, B describes a second-order deviation from linear growth; A and α parametrize the power law that dominates the function in the quasi-linear regime; V is the virialization parameter that gives the amplitude of the $f_{\rm NL}(x) \propto x^{3/2}$ asymptote (where the behavior enters the "stable clustering" limit); and β softens the transition between these regimes. For power spectra of the form $|\delta^2_k| \propto k^n$, the parameters and their dependence on n are

$$\begin{aligned} A &= 0.482(1 + n/3)^{-0.947} \,, \\ B &= 0.226(1 + n/3)^{-1.778} \,, \\ \alpha &= 3.310(1 + n/3)^{-0.244} \,, \\ \beta &= 0.862(1 + n/3)^{-0.287} \,, \\ V &= 11.55(1 + n/3)^{-0.423} \,. \end{aligned} \tag{11}$$

The growth factor, $g(\Omega)$, is proportional to the ratio of the linear growth factor to the expansion factor. It takes the value unity for $\Omega = 1$, and, for $\Omega_0 < 1$, it tends to unity as $\Omega \to 1$.

For linear spectra that are not a power law, particularly for the CDM model, Peacock & Dodds (1996) suggested that a tangent spectral index as a function of linear wavenumber should be used:

$$n_{\rm eff}(k_L) \equiv \frac{d\ln P}{d\ln k}\,(k = k_L/2) \,. \tag{12}$$

The factor of 2 shift to smaller k is required because the tangent power law at $k_{\rm L}$ overestimates the total degree of nonlinearity for curved spectra in which $n_{\rm eff}$ is a decreasing function of k and underestimates it in the opposite case. Peacock & Dodds (1996) state that this prescription is able to predict the nonlinear evolution of power-law and CDM spectra up to $\Delta^2 \simeq 10^3$ with an rms precision of about 7%. Since the fitting formula is designed to reproduce the results for power-law spectra, the main uncertainty in this method is whether or not the shifted tangent power law is the best means of deducing the effective n as a function of scale. This issue becomes especially important when the effective index is more negative than -2 (because nonlinear effects diverge as $n \to -3$) and when the curvature of the spectrum is especially severe. This means that spectra with low values of $\Omega_0 h$ or of σ_8 present the greatest challenge for the analytic method.

The effect of cosmology enters into the fitting formula only through the growth factor, $g(\Omega)$, which governs the amplitude of the virialized portion of the spectrum.

7.2. *Fit to the Simulations*

The nonlinear power spectrum predicted by equation (11) for each of our four cosmological models is plotted as a solid line in Figure 7. The solid circles and crosses show the results from our large- and small-volume simulations, respectively. Note the excellent agreement between them. The dashed curve shows the linear theory prediction for the present-day power spectrum.[11] The points are plotted only on scales where the power exceeds the shot noise. The agreement between the analytical and numerical results is generally good, particularly for SCDM and ΛCDM. For all the models with $\Gamma = 0.21$, the predicted power spectrum slightly underestimates the detailed power spectrum of the simulations around the region $\Delta^2 \simeq 10$. As discussed above, these cases are expected to be especially challenging because they have a more negative $n_{\rm eff}$ at the nonlinear scale. The slight mismatch illustrates the difficulty in defining precisely the effective power-law index for these rather flat spectra, and a more accurate formula could be produced for this particular case, if required. Note that in the quasi-linear portion the power spectra follow very closely the general shape predicted by equations (8)–(12); in particular, there is essentially no difference between the OCDM and ΛCDM results, as expected.

The power spectra of the different cosmological models are expected to part company at higher frequencies, where the spectrum enters the "stable clustering" regime, and indeed they do. However, although the predictions match the ΛCDM results almost precisely at $\Delta^2 \simeq 1000$, they lie above the OCDM results at high k: $\Delta^2(k = 30) \simeq 4500$, compared to the simulation value of 2500. At one level, this is not so surprising, since the smaller simulations that Peacock & Dodds (1996) used to derive the parameters of the fitting formula were not able to resolve scales beyond $\Delta^2 \simeq 1000$. However, the amplitude of the stable clustering asymptote is very much as expected in the $\Omega = 1$ and ΛCDM cases, and the argument for how this amplitude should scale with Ω_0 is straightforward: at high redshift,

[11] The realization of the power spectrum in our simulations can be seen to have a downward fluctuation in power at $1 \leq |kL/2\pi| < 2$, where L is the simulation box size. A χ^2 test for these 26 modes shows that a fluctuation lower than this is expected in 7% of cases. While this fluctuation is not particularly unusual, it has little effect on the results of interest (except for bulk flows; see §§ 3.1, 5, and 8) because our simulated volumes are sufficiently large.

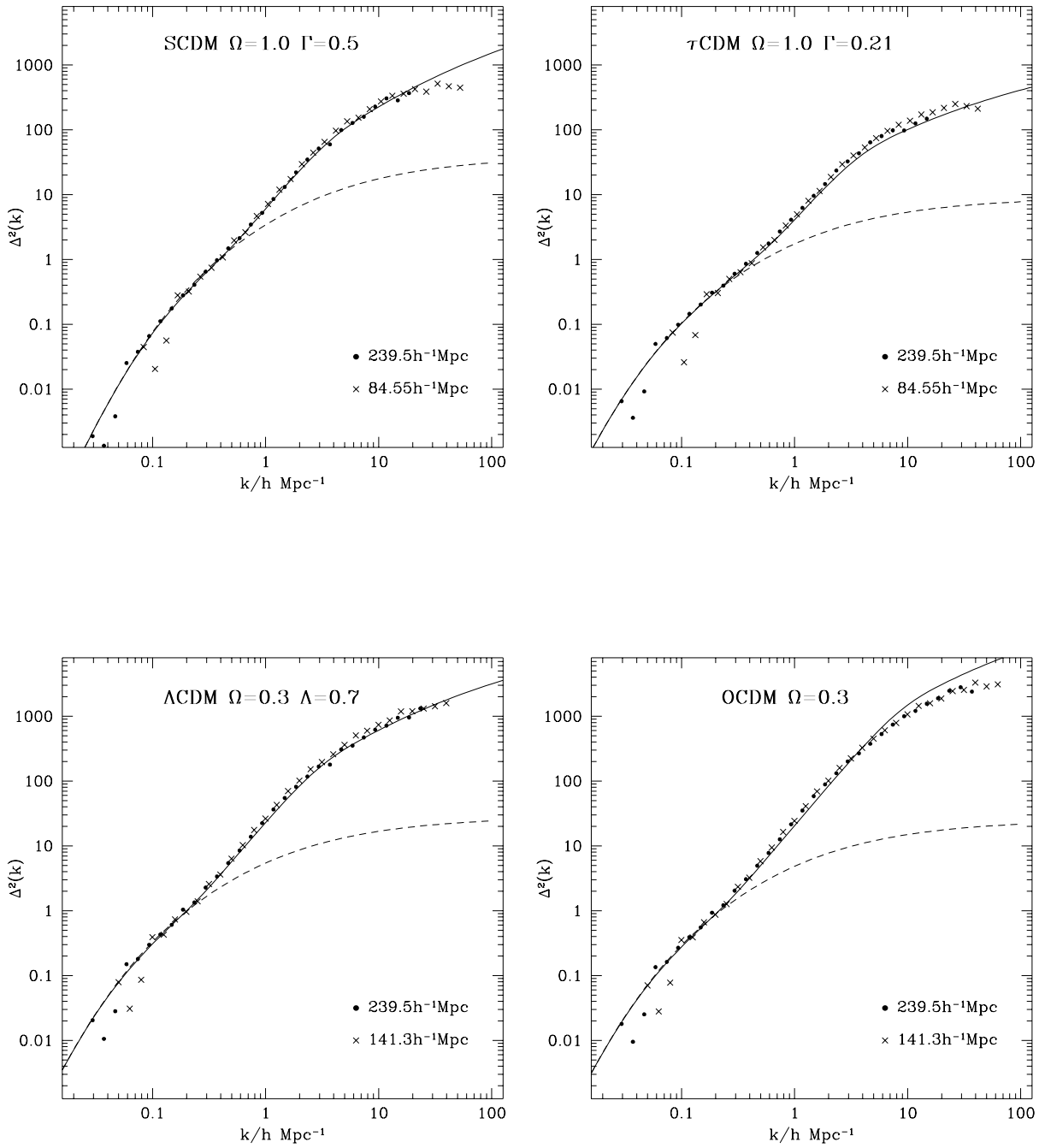

FIG. 7.—Predicted nonlinear power spectra at $z = 0$ compared with N-body simulation results. The analytical results for our four cosmological models are shown as solid curves, and the N-body results in our large- and small-volume simulations are shown by filled circles and crosses, respectively. The dashed line shows the linear theory prediction for the power spectrum at $z = 0$. At small wavenumbers, the simulations depart from the linear theory curve because of the small number of modes in each bin.

clustering in all models evolves as in an $\Omega = 1$ universe, and so evolution to the present is determined by the balance between the linear growth rate and the (Ω_0-independent) rate of growth of stable clustering. The failure of this scaling for the OCDM case is therefore something of a puzzle. It is conceivable that the numerical result could be inaccurate, since it depends on resolving small groups of particles with overdensities of several thousand, and these collapse very early on. However, we have verified that changing the starting redshift from 59 to 119 does not alter the results of the simulations significantly.

Figure 8 shows the two-point correlation function derived using equation (7) and the predicted nonlinear power spectrum, equations (8)–(12). As before, the N-body results are plotted as filled circles and crosses for the large- and small-volume simulations, respectively. Note that, in general, the agreement between each pair of simulations is very good, and the very small discrepancies that there are can be understood simply. At large pair separations, $\xi(r)$ is slightly depressed in the smaller simulations because these separations are becoming an appreciable fraction of the box length and the integral constraint requires $\xi(r)$ to average to

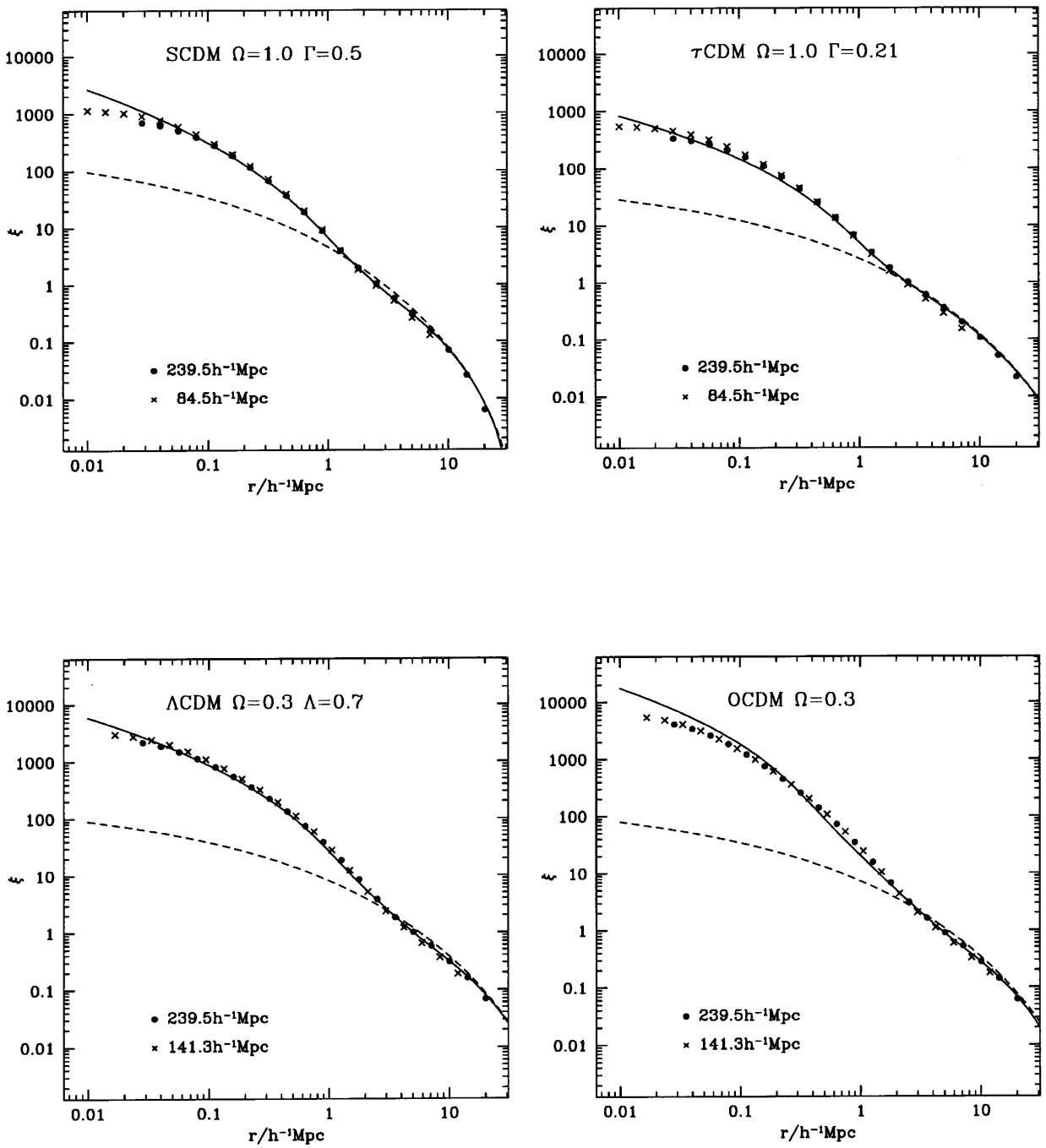

FIG. 8.—Predicted mass correlation functions at $z = 0$ compared with N-body simulation results. The analytical results for our four cosmological models are shown as solid curves, and the N-body results in our large- and small-volume simulations are shown by filled circles and crosses, respectively. The dashed line shows the linear theory prediction for $\xi(r)$ at $z = 0$. At large pair separations, the integral constraint in the smaller simulations depresses $\xi(r)$ slightly, whereas at small pair separations, $\xi(r)$ is slightly higher in the smaller volumes because they have better mass resolution.

zero over the volume of the simulation. At small pair separations, $\xi(r)$ is slightly higher in the smaller volumes because of their higher mass resolution. Once again, there is good agreement in general between the analytical predictions and the N-body results, particularly for the ΛCDM and SCDM models. For τCDM, the model underpredicts the correlation function on scales below 700 h^{-1} kpc, while for OCDM, the model correlation function is somewhat steeper than in the simulations. These differences occur on scales significantly larger than those affected by resolution effects and are fully consistent with the analogous deviations seen in the power spectrum.

8. THE VELOCITY FIELDS AND DISTRIBUTIONS

In this section we compute bulk flows, velocity dispersions, and pairwise velocities of the dark matter particles in our simulations. Potentially, measurements of galaxy peculiar velocities can provide powerful tests of the models. In practice, there are a number of complications that weaken these tests. Foremost among them is the uncertain relation between the velocity fields of dark matter and galaxies, particularly on small scales where various dynamical biases may operate (Carlberg et al. 1990; Frenk et al. 1996). It is relatively straightforward to calculate, with high precision,

the velocity fields of the dark matter in a given cosmology, using simulations like ours or, in the appropriate regime, using linear theory. To relate these to observations on small scales requires an understanding of possible dynamical biases and, in the case of pair-weighted statistics, of sampling uncertainties and systematic effects arising from the discrete nature of the galaxy population. Only on sufficiently large scales do we expect galaxy bulk flows that are, in principle, measurable to be simply related to the dark matter bulk flows.

Observational determinations of galaxy velocities have their own complications. For example, determining bulk flows over representative volumes requires measuring peculiar velocities, and thus determining distances with an accuracy of a few percent, for large samples of galaxies. Defining such samples in a homogeneous way and keeping systematic effects in the distance measurements within tolerable levels is a complex and still uncertain process (e.g., Willick et al. 1997). Other measures of the galaxy velocity field such as the pairwise relative velocities of close pairs are also affected by systematic and sampling effects, even though they do not require measuring distances (e.g., Marzke et al. 1995; Mo et al. 1996).

In view of the various uncertainties just mentioned, we focus here on high-precision estimates of various measures of the dark matter velocity field. Our main purpose is to contrast the velocity fields predicted in the four cosmological models considered in this paper, in the expectation that these and related calculations may eventually be applied to a reliable interpretation of real galaxy velocity fields. We do, however, carry out a limited comparison of dark matter velocity fields with existing data on large-scale galaxy bulk flows and pairwise velocity dispersions. In § 8.1 we compute distributions of the mean and rms dark matter velocity on various scales, and in § 8.2 we consider pairwise velocities also over a range of scales.

8.1. *Bulk Flows and Dispersions*

We compute bulk flows and velocity dispersions of dark matter particles in the simulations by placing a large number of spheres of varying radii around random locations in the computational volume. We define the bulk velocity of a sphere as

$$\boldsymbol{V} = \frac{1}{N} \sum_{i=1,N} \boldsymbol{v}_i \,, \tag{13}$$

where $\boldsymbol{v}_i$ is the peculiar velocity of the ith particle out of N in a given sphere, and all particles have equal weight. The dispersion, σ_v, is defined as

$$\sigma_v^2 = \frac{1}{N-1} \sum_{i=1,N} (\boldsymbol{v}_i - \boldsymbol{V})^2 \,. \tag{14}$$

In linear theory, the bulk velocity of the dark matter can be accurately calculated according to

$$\langle V^2 \rangle = \Omega_0^{1.2} \int_0^\infty k^{-2} W^2(Rk) \Delta^2(k) \frac{dk}{k} \,, \tag{15}$$

where $W(Rk)$ is a window function, which we take to be a top hat of radius R in real space. The approximate factor $\Omega_0^{1.2}$ works well for all the cosmological models we are considering here (Peebles 1980).

The integral in equation (15) ranges over all spatial scales and so applies to a simulation only in the limit of an infinite volume. In order to compare the simulations with linear theory, it is necessary to take account of effects due to the finite computational box and of the fact that we have only one realization. Finite box effects are much more significant for velocities than for the correlation function (eq. [6]), since the relative importance of longer waves is enhanced in equation (15) by a factor k^{-2}. To compare linear theory with a specific simulation, the integral in expression (15) must be replaced by a summation over the modes of the periodic box, using the appropriate power in each mode as set up in the initial conditions.

The dashed curve in Figure 9 shows the linear theory prediction for bulk flows at $z = 0$, in spheres of radius $R_{\rm sphere}$, for a model with the power spectrum and normalization of our τCDM simulation, in the limit of infinite volume. The predicted velocities fall off smoothly from about 500 km s^{-1} at 10 h^{-1} Mpc to about 200 km s^{-1} at 100 h^{-1} Mpc. The dotted curve shows the linear theory ensemble average value of $\langle V^2 \rangle^{1/2}$ over realizations of the τCDM power spectrum in volumes the size of our simulation. The difference between this and the dashed curve indicates just how important finite box effects are in computing bulk flows. The error bars on the dotted curve show the rms dispersion among different realizations. For small spheres, the variation about the mean is approximately Gaussian, and the error bars may be regarded as 1 σ deviations from the mean. The results from our actual simulation at $z = 0$ are plotted as solid circles in the figure, and the linear theory prediction for evolution from the specific initial conditions of this simulation is shown as the solid curve. The particular realization that we have simulated turned out to produce slightly, but not anomalously, low velocities. On scales above 20 h^{-1} Mpc, the linear theory prediction

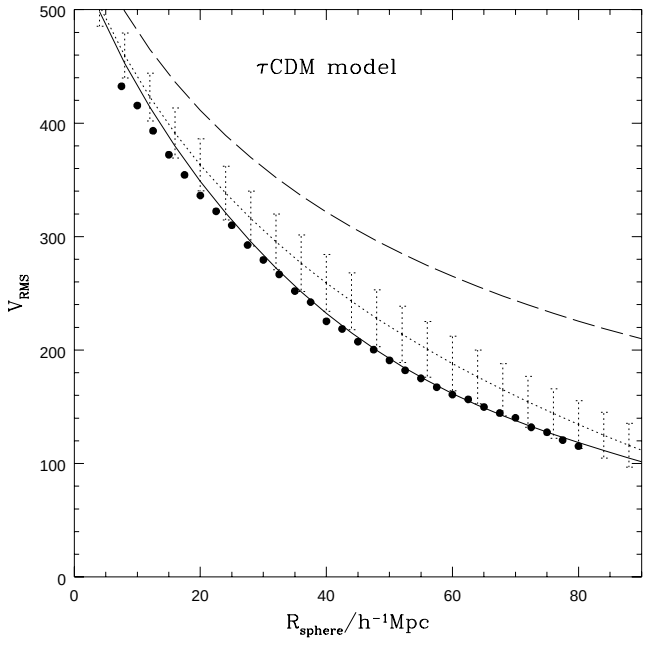

FIG. 9.—Comparison of the bulk flow measured in the τCDM model (*solid circles*) with linear theory. The long-dashed curve is the linear theory result in the limit of an infinite box size. The dotted line with error bars shows the ensemble rms average for a 239.5 h^{-1} Mpc periodic box. The error bars give the rms spread between different realizations. The solid line is the result from linear theory for the realization used in our τCDM simulation. Linear theory works to excellent approximation when all the finite box effects are taken into account.

agrees very well with the simulation; at $R = 10\ h^{-1}$ Mpc, it overestimates the actual velocities by 5%.

While linear theory suffices to calculate bulk flows on scales larger than about $10\ h^{-1}$ Mpc, the velocity dispersion of particles in spheres is dominated by contributions from nonlinear scales and must be obtained from the simulations. Finite box effects are not important in this case because the contributions from wavelengths larger than the simulation box are small.

The bulk flows, $\langle V^2 \rangle^{1/2}$, calculated from linear theory and the velocity dispersions in spheres, σ_v, calculated from our $L = 239.5\ h^{-1}$ Mpc simulations are plotted as solid lines in Figure 10 for our four cosmological models. The dotted curves around the $\langle V^2 \rangle^{1/2}$ curve correspond to 90% confidence limits on the bulk velocity for a randomly placed sphere, calculated by integrating over the appropriate Raleigh distribution. The dotted curves around the σ_v curve indicate the rms scatter of the σ_v distribution.

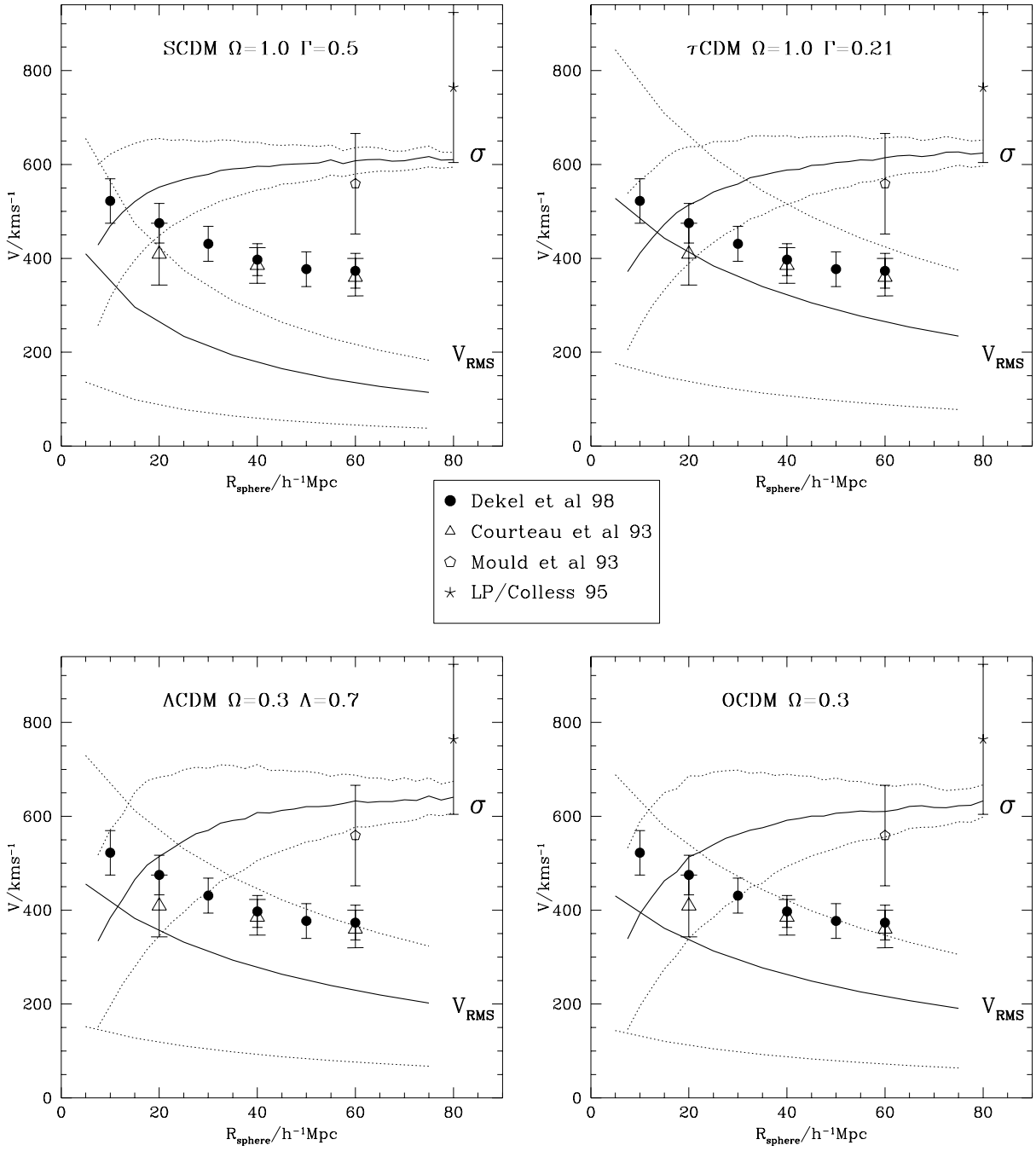

FIG. 10.—Dark matter bulk flows and velocity dispersions in spheres of different radii. The bulk flows, computed from linear theory, are shown by the lower solid line, with 90% confidence limits indicated by dotted lines. The rms velocity dispersions, computed from the simulations, are shown by the upper solid curve, with the rms scatter indicated by the dotted lines. The data points with error bars are observational estimates of galaxy bulk flows from Dekel et al. (1998), Courteau et al. (1993), Mould et al. (1993), and Lauer & Postman (1993), as reanalyzed by Colless (1995) (see legend in the middle of the figure). The predicted velocity fields are very similar in all the models because they are normalized to give the same abundance of rich clusters. The only exceptions are the predicted bulk flows in the SCDM model, which are slightly smaller than in the other models because of its different power spectrum shape. Every model except SCDM is consistent with the galaxy bulk flow data, with the exception of the Lauer & Postman result.

With the exception of SCDM, the predicted bulk flows in all of our models are remarkably similar. The reason for this can be traced back to our choice of normalization, which ensures that all models produce approximately the same number of rich galaxy clusters. This choice effectively cancels out the dependence of the bulk flow velocity on Ω_0 as may be seen directly from linear theory. From equation (15), $\langle V^2 \rangle^{1/2} \propto \sigma_8 \Omega_0^{0.6}$ for a fixed shape of the power spectrum. On the other hand, our adopted fluctuation normalization requires approximately that $\sigma_8 \propto \Omega_0^{-0.5}$ (see eqs. [1] and [2]). Since the power spectra of the ΛCDM, τCDM, and OCDM models all have the same shape parameter, $\Gamma = 0.21$, the bulk flows in these models are very similar. The lower bulk flow velocities predicted in the SCDM model reflect the relatively smaller amount of large-scale power in this model implied by its value of $\Gamma = 0.5$. The mean bulk velocity in SCDM is approximately two-thirds of the value in the other models.

The peculiar velocity dispersion of dark matter particles in random spheres is also remarkably similar in all of our models, including SCDM. In this case, significant contributions to σ_v come from a wide range of scales, including nonlinear objects as well as regions that are still in the linear regime. On small scales, σ_v rises with increasing sphere radius and reaches a plateau at radii of a few tens of megaparsecs. The limit as the radius tends to infinity is just the single-particle rms peculiar velocity. For our large simulation boxes, this is 614, 635, 648, and 630 km s^{-1} for the SCDM, τCDM, ΛCDM, and OCDM models, respectively. The slightly lower value for SCDM again reflects the smaller large-scale power in this model compared to the others. This deficit on large scales, however, is compensated by an excess contribution from smaller scales.

We have plotted in Figure 10 estimates of galaxy bulk flow velocities in the local universe taken from the analyses by Mould et al. (1993), Courteau et al. (1993), Dekel et al. (1998), and Lauer & Postman (1994). These estimates are based on different data sets and assumptions, and, apart from the Lauer & Postman measurement, they are broadly consistent with one another, although the Mould et al. measurement is somewhat high. The data from the first three surveys are broadly consistent with the predictions of all of our models except SCDM, which produces velocities about a factor of 2 lower than the data on large scales. None of the models is consistent with the measurement of Lauer & Postman, who inferred a bulk flow of 764 ± 160 km s^{-1} (as reanalyzed by Colless 1995) on a scale of $\sim 80\ h^{-1}$ Mpc from a sample of brightest cluster galaxies. The results in the figure show that bulk flows are insensitive to the value of Ω_0 when one focuses attention on models that agree with the observed cluster abundance. If anything, observed bulk flows constrain the shape of the power spectrum on large-scales, or, in the case of the Lauer & Postman result, they conflict with the entire class of models we are considering.

8.2. *Pairwise Velocities*

We now consider the lower order moments of the pairwise velocity distribution of dark matter particles in our four cosmological models. Specifically, we consider the following quantities: v_{21}, the mean radial peculiar velocity of approach between particle pairs; $v_\parallel^2$, the dispersion in the radial velocities of pairs; and $v_\perp^2$, the dispersion in the mean transverse relative velocities of pairs. Following standard practice, $v_\parallel^2$ is not centered; to center one just needs to subtract v_{21} in quadrature. These quantities are not directly observable, but we also compute the dispersion, $\sigma_{\rm los}^2$, the line-of-sight velocity dispersion (this time centered), defined as

$$\sigma_{\rm los}^2(r) = \frac{\int \xi(R)\sigma_{\rm proj}^2(R)dl}{\int \xi(R)dl}\,, \tag{16}$$

where r is the projected separation, $R = (r^2 + l^2)^{1/2}$, and the integral is taken along the line-of-sight between $\pm 25\ h^{-1}$ Mpc. The quantity $\sigma_{\rm proj}^2$ is the line-of-sight centered pairwise dispersion, which is given by

$$\sigma_{\rm proj}^2 = \frac{r^2 v_\perp^2/2 + l^2(v_\parallel^2 - v_{21}^2)}{r^2 + l^2}\,. \tag{17}$$

This quantity is somewhat closer to measurements accessible in galaxy redshift surveys; it is a much weaker function of apparent separation than $v_\parallel^2$ and $v_\perp^2$.

Figure 11 shows v_{21}, $v_\parallel$, $v_\perp$, and $\sigma_{\rm los}$ as a function of pair separation in our models. Also drawn on each panel is the Hubble line, given by $v_{\rm Hubb} = -Hr$, where H is Hubble's constant, and r is pair separation in physical units. Pairs at fixed physical separation lie on this line. In the stable clustering regime (Peebles 1980), v_{21} must follow $v_{\rm Hubb}$. The distance at which the mass correlation function equals unity, the correlation length, is marked by an arrow.

The mean pairwise radial velocities, v_{21}, vanish at the smallest separations resolved in our simulations. In the low-Ω_0 models, where the growth of structure is freezing out at low redshift, v_{21} follows the Hubble line up to scales $\sim 300\ h^{-1}$ kpc. This indicates that structures on these scales have almost completely relaxed, and the clustering is stable. In the $\Omega = 1$ models there is still a net radial inflow on these scales, although the inflow timescale is longer than the Hubble time and very much longer than the local dynamical time of pairs at these separations [where $\xi(r) = 80 - 200$]; the latter is, in turn, much shorter than the Hubble time. The pairwise radial velocity in these models reaches a peak inside the correlation length (marked by the arrow), around 2–3 h^{-1} Mpc. This indicates the typical scale of virializing structures at $z = 0$ in the $\Omega = 1$ models. At larger radial separations v_{21} intersects the Hubble line and, at very large separations, it decays to zero, in accordance with the principle of large-scale isotropy and homogeneity.

For the same reasons, one expects the ratio $v_\perp^2/v_\parallel^2$ to tend to $\sqrt{2} = 1.414$ at large separations. The measured ratios at a separation of $80\ h^{-1}$ Mpc are 1.38, 1.34, 1.36, and 1.37 for SCDM, τCDM, ΛCDM, and OCDM. At scales of a few h^{-1} Mpc, where radial infall is at its most important, the ratio in the SCDM model is about 1.23 (after centering). At smaller scales still, the relative motions inside virialized structures again become closer to isotropy, in agreement with results from high-resolution simulations of dark halos (Tormen 1996; Thomas et al. 1997). On very small scales, two-body effects contribute to the isotropization of the orbits.

As was the case with the mean bulk flows and velocity dispersions in random spheres discussed in § 8.1, the moments of the pairwise velocity distribution are very similar in the different cosmologies. As before, this similarity is a direct consequence of our adopted normalization. The largest differences occur between the OCDM and τCDM models on small scales—a difference of about 200

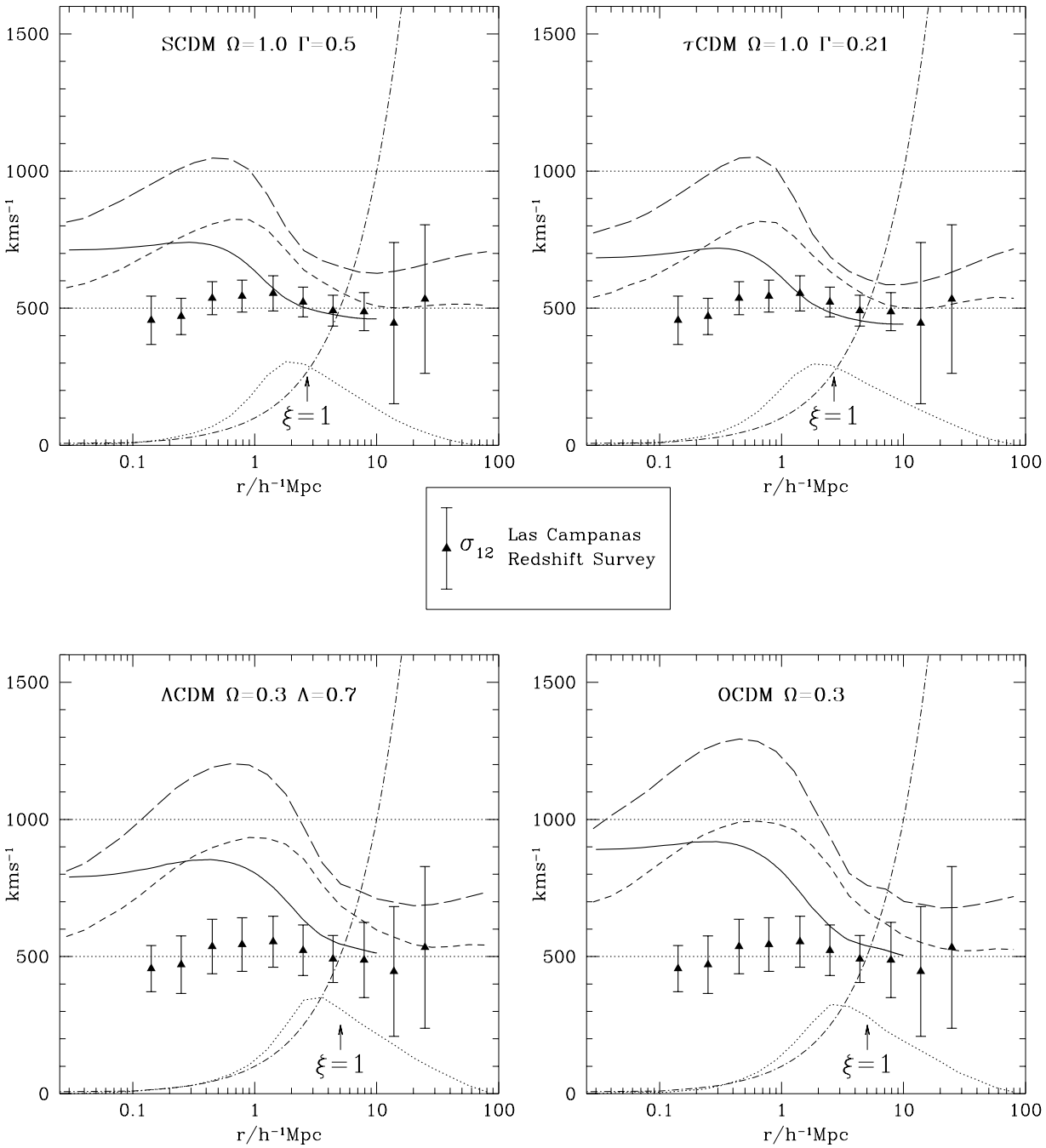

FIG. 11.—Pairwise velocity statistics. In each panel, the dotted curve is the mean inward radial velocity, v_{21}; the short dashed line is the dispersion in the pairwise radial peculiar velocities, $v_{\|}$; the long dashed line is the dispersion in the relative pairwise tangential peculiar velocities, $v_{\perp}$; the solid line is the line-of-sight dispersion, $\sigma_{\rm los}$; and the dot-dashed line is the Hubble line given by $v_{\rm Hubb} = -Hr$, where H is Hubble's constant, and r is physical separation. The dispersion, $v_{\|}$, is uncentered; to center, subtract v_{21} in quadrature. The data points are taken from Jing et al. (1997) and show the pairwise velocity dispersion, σ_{12}, estimated for the Las Campanas redshift survey. These points should be compared to the line-of-sight dispersions for the models. See the text for discussion of the error bars used on these points.

km s^{-1} in $\sigma_{\rm los}$. Qualitatively, the trends seen in Figure 11 agree with the analytical calculation of Mo et al. (1996), who find that pairwise velocities in open models are slightly larger than in Λ models, and these, in turn, are larger than in $\Omega = 1$ models.

It is difficult to compare the predicted dark matter pairwise velocities with galaxy measurements for a variety of reasons. First, the velocity dispersion of the dark matter distribution in the simulations includes a contribution from the internal dispersion of virialized halos. Second, there is some evidence that the velocity dispersion of dark halos in simulations may be biased low relative to the dark matter velocity dispersion even after allowing for contamination from virialized halos (Carlberg & Couchman 1989), an effect that Carlberg et al. (1990) argue is due to dynamical friction (see also Zurek et al. 1994). (The velocities of the dark matter halos in our simulations will be analyzed in a future paper by Frenk et al. 1998.) Finally, biases in the spatial distribution of galaxies may introduce further biases in the pairwise velocity statistics of the galaxies relative to

the dark matter (Fisher et al. 1994; Weinberg 1995; Evrard, Summers, & Davis 1994).

Observationally, the velocity dispersion of galaxy pairs is determined by fitting a model under certain assumptions regarding the two-point correlation function and the spatial dependence of the infall velocity and dispersion (Davis & Peebles 1983). These assumptions do not necessarily match the simulation data. More importantly, as Marzke et al. (1995) and Mo et al. (1996) have argued, pairwise velocity statistics are not robust when determined from relatively small redshift surveys since these statistics contain significant contributions from galaxy pairs in rare, massive clusters. This is not a problem in our simulations, which sample a volume of 13.8×10^6 $(h^{-1}$ Mpc$)^3$, but it is a problem in the present generation of redshift surveys with the possible exception of the Las Campanas Redshift Survey (Shectman et al. 1996, hereafter LCRS). Estimates of the pairwise velocity dispersion in the LCRS, obtained by Jing et al. (1997), are shown as data points in Figure 11. The LCRS contains quite a number of rich clusters and appears to give consistent estimates when split into northern and southern subsamples. The error bars plotted in the figure are the sum in quadrature of the errors obtained directly from the data by Jing et al. (1997) plus the 1 σ uncertainties found from applying the same estimator to mock catalogues constructed from N-body simulations by these authors. The LCRS velocities are substantially larger than most previous determinations. The dispersion remains approximately constant over the range 0.15–10 h^{-1} Mpc, reaching an amplitude of 570 ± 80 km s^{-1} at 1 h^{-1} Mpc.

The LCRS data may be compared with the line-of-sight dispersions plotted for each of our simulations in Figure 11. At pair separations $\gtrsim 2$ h^{-1} Mpc, all of our models are consistent with the data, although the low-Ω models lie somewhat low. At smaller separations, all model curves rise above the data. This difference in behavior may be due, in part, to the different methods for estimating the dispersion in the simulations and the data, but it very likely reflects also the biases present in the simulations mentioned earlier. Interestingly, the $\Omega = 1$ models are closer to the data on small scales than the low-Ω models, which implies that substantially stronger velocity biases are required in low-Ω models to bring them into agreement with the data.

9. DISCUSSION AND CONCLUSIONS

We have used a suite of high-resolution N-body simulations to investigate the clustering evolution of dark matter in four different cold dark matter cosmologies. Our simulations followed approximately 17 million particles. Most of our analysis is based on simulations of very large cosmological volumes (239.5 h^{-1} Mpc$)^3$, but we also analyzed simulations of somewhat smaller volumes and correspondingly higher mass resolution. The large volumes and particle numbers, together with a relatively small gravitational softening (~ 30 h^{-1} kpc), allow us to calculate the clustering and kinematical properties of the dark matter with unprecedented accuracy. For example, we are able to determine the mass autocorrelation function over nearly three decades in pair separation with better accuracy than in previous simulations and also with higher precision than is attainable with existing or planned surveys of galaxies. Our model mass correlation functions are well fit by an analytic model of the type proposed by Hamilton et al. (1991) but with the form and parameters proposed by Peacock & Dodds (1996). This model may therefore be used to extend some of the results of our analysis to cosmologies with different parameter values to those assumed in our simulations.

Two of the four variants of the CDM cosmology that we have investigated are motivated by various lines of astronomical evidence that suggest a low cosmological density parameter, $\Omega_0 \simeq 0.3$, and a spectral shape parameter, $\Gamma = 0.21$; we study both a flat model with a non-zero cosmological constant (ΛCDM) and an open model (OCDM). The remaining two models both have $\Omega = 1$, but one has the standard power spectrum (SCDM), and the other has $\Gamma = 0.21$ (τCDM). In all cases, we have chosen to normalize the primordial fluctuation spectrum so that the present abundance of rich clusters is approximately reproduced in all the models. We regard this choice as preferable to the often used alternative of normalizing to the amplitude of the *COBE* microwave background anisotropies. With standard assumptions (a Harrison-Zeldovich primordial spectrum and no contribution to the anisotropy from tensor modes), the cluster normalization is close to the *COBE* normalization for the ΛCDM and τCDM models, but it is significantly higher for the OCDM and significantly lower for the SCDM model. With our choice of normalization, the overall appearance of all models is determined primarily by their σ_8 values with the result that the two high-density models look very similar, while the two low-density models show more structure but resemble each other closely.

Our main results concern the detailed properties of the spatial distribution and velocity fields of the dark matter at $z = 0$. We now discuss our results and display them concisely in Table 2. In all of the models, the shape of the two-point correlation function, $\xi(r)$, and power spectrum, $\Delta^2(k)$, of the dark matter differ significantly from those of the observed galaxy distribution. In particular, they fail to reproduce the accurate power law which the APM survey (and others before that; cf. Groth & Peebles 1977) exhibits over nearly 4 orders of magnitude in amplitude. At small,

TABLE 2

SUMMARY OF RESULTS

Model[a]	Cluster Abundance	*COBE* Normalization	Constant Bias	Small-Scale Bias/Antibias	$V_{\rm bulk}$[b]	Pairwise Velocities
SCDM	Yes	No	No	Bias	Low	Slightly high
τCDM.....	Yes	Yes	Yes	Bias	OK	Slightly high
ΛCDM	Yes	Yes	No	Antibias	OK	High
OCDM.....	Yes	No[c]	No	Antibias	OK	High

[a] See Table 1 for the definitions of the models.

[b] When compared to the data plotted in Fig. 10, with the exception of the Lauer & Postman (1994) measurement. All of our models are strongly inconsistent with the latter.

[c] A model with Ω_0 in the range 0.4–0.5 and a slightly lower value of h agrees with both the cluster abundance and *COBE*-DMR constraints.

but still well-resolved pair separations, all of our model correlation functions become shallower, while at intermediate separations, they all have an inflection point. Uniquely among the models we have explored, τCDM has a mean correlation slope that is approximately correct over the bulk of the observable range, but even in this case there are substantial discrepancies on scales smaller than $\sim 0.2\ h^{-1}$ Mpc. Thus, for any of these models to provide an acceptable representation of reality, the distribution of galaxies would need to be biased relative to the mass in a nontrivial, scale-dependent fashion. Whatever the processes involved in biasing the galaxy distribution may be, they must conspire to iron out the features in the dark matter correlation function.

We define a "bias function" as the square root of the ratio of the galaxy to the mass autocorrelation functions. Our simulations, together with the galaxy autocorrelation function measured from the APM survey by Baugh (1996), give the bias as a function of scale accurately for the four models we have investigated. We find that our two $\Omega = 1$ models require a bias greater than unity everywhere. In the SCDM case, the bias grows from ~ 1 at $\sim 1\ h^{-1}$ Mpc to ~ 1.5 at $\sim 8\ h^{-1}$ Mpc and rises sharply beyond that. In the τCDM model, the bias is approximately constant, at $b \simeq 1.5$, between ~ 0.2 and $\sim 20\ h^{-1}$ Mpc.

By design, our low-Ω_0 models have a power spectrum that approximates that of the APM galaxy survey on large scales. However, even in this case, the match is not perfect, and some amount of bias may still be required at separations greater than $10\ h^{-1}$ Mpc. Furthermore, these models have the undesirable feature that the mass correlation function rises above the APM galaxy correlation function at pair separations smaller than $\sim 5\ h^{-1}$ Mpc. On these scales, an "antibias" is required for these models to match the observed galaxy clustering. Galaxy mergers in high-density regions may plausibly suppress small-scale correlations, but it remains to be seen whether an antibias of the required magnitude is achievable in practice. Antibiasing may be difficult to reconcile with observed cluster mass-to-light ratios. In standard virial analyses of clusters, a value of Ω_0 is derived from the measured mass-to-light ratio by assuming that the galaxies cluster just like the mass. With this assumption Carlberg et al. (1997), for example, inferred $\Omega_0 = 0.19 \pm 0.06$ from the Canadian Network for Observational Cosmology (CNOC) sample of intermediate redshift clusters. If galaxies were actually antibiased, this estimate of Ω_0 would need to be corrected downward. However, models with lower values of Ω_0 require higher values of σ_8, and even stronger antibias, in order to reproduce the observed abundance of clusters.

Our simulations allow us to calculate accurately the velocity fields of the dark matter over a wide range of scales. These are very similar in all of our models, whether they be characterized as bulk flows, single-particle, or pairwise velocity dispersions. This similarity in the velocity fields is a direct consequence of our adopted normalization and runs contrary to the common belief that the amplitude of the observed galaxy velocity fields can be used to constrain the value of Ω_0. A residual dependence of the velocity field on the shape of the power spectrum causes the velocities in the SCDM model to be somewhat lower than in the other models, but among the latter there is no discernible difference. For example, the one-dimensional velocity dispersion of the dark matter is approximately 600 km s^{-1} in all the models, and the line-of-sight pairwise velocity dispersions fall in the range 700–900 km s^{-1}. The first of these numbers is reminiscent of the peculiar velocity of the Local Group, while the second is consistent with, although on the high side of, a recent determination from the Las Campanas redshift survey at a pair separation of $\sim 1\ h^{-1}$ Mpc (Jing et al. 1997). On smaller scales, our simulations, particularly our low-Ω_0 models, predict higher pairwise velocity dispersions than inferred from this survey, which indicates that a substantial velocity bias is required to bring the models into agreement with the data. Bulk flows on large scales are most accurately calculated using linear theory. Our models all predict somewhat smaller values than those estimated from recent surveys of the local universe (Mould et al. 1993; Courteau et al. 1993; Dekel et al. 1998), but, with the exception of SCDM, they are consistent with these data. None of the models reproduces the large bulk flows inferred by Lauer & Postman (1994).

High-resolution simulations like those presented here allow very accurate measurements of the clustering distribution of dark matter. Further progress in this subject will rely on the ability to address the outstanding issue that limits the comparison of these models with observations: the connection between the distribution of mass and the distribution of galaxies. This will require a realistic treatment of the evolution of the baryonic component of the universe.

We are grateful to Carlton Baugh for useful discussions and for providing us with the APM galaxy survey data used in Figures 5 and 6. We thank David Weinberg for suggesting several significant improvements to the manuscript and Avishai Dekel for communicating to us, in advance of publication, results of his bulk analysis shown in Figure 10. C. S. F. acknowledges a PPARC Senior Fellowship. This work was supported in part by grants from PPARC, EPSRC, and the EC TMR network for "Galaxy Formation and Evolution." The simulations reported here were carried on the Cray-T3Ds at the Edinburgh Parallel Computing Centre and the Rechenzentrum, Garching. We thank the editor for suggesting the inclusion of Table 2.

APPENDIX

Derivation of Equation (5)

The two-point correlation function is related to the power spectrum by

$$\xi(\boldsymbol{r}) = \int P(\boldsymbol{k}) \exp\,(i\boldsymbol{k} \cdot \boldsymbol{r}) d^3\boldsymbol{k}\ , \tag{A1}$$

where the bold italic font implies that the quantity is a three-dimensional vector.

In deriving a correction to the linear correlation function for a periodic box, we must make an assumption for how the power selected for each discrete mode of the periodic box is related to the power density of the same mode in the continuous power spectrum. As discussed in § 3.1, we draw the power for each mode from an exponential distribution with the mean power set by the power density of the mode in the continuous power spectrum. Thus, the ensemble-average linear correlation function of the periodic boxes, $\xi_s(\boldsymbol{r})$, is given by

$$\xi_s(\boldsymbol{r}) = \left(\frac{2\pi}{L}\right)^3 \sum_{\boldsymbol{b}=(0,0,0)}^{\infty} P\left(\frac{2\pi \boldsymbol{b}}{L}\right) \exp\,(2\pi i \boldsymbol{b}\cdot\boldsymbol{r}/L)\,, \tag{A2}$$

where L is the simulation box size, and the sum over $\boldsymbol{b}$ is a sum over all integer triples. The correction we derive is a systematic correction that applies to an ensemble of simulations.

We make use of the Poisson summation formula which, for a function $\phi(\boldsymbol{x})$, states that

$$\sum_{\boldsymbol{b}=(0,0,0)}^{\infty} \phi(2\pi \boldsymbol{b}) = \frac{1}{(2\pi)^3} \sum_{\boldsymbol{n}=(0,0,0)}^{\infty} \int \phi(\boldsymbol{t}) \exp\,(i\boldsymbol{n}\cdot\boldsymbol{t}) d^3\boldsymbol{t}\,, \tag{A3}$$

subject to certain conditions on the function $\phi(\boldsymbol{x})$ which hold for the case of interest here (see Courant & Hilbert 1953, p. 76).

Substituting the right-hand side of equation (A2) into the Poisson summation formula, we obtain

$$\xi_s(\boldsymbol{r}) = \sum_{\boldsymbol{n}=(0,0,0)}^{\infty} \int P(\boldsymbol{k}) \exp\,[i\mathbf{k}\cdot(\boldsymbol{r} - L\boldsymbol{n})] d^3\boldsymbol{k}\,. \tag{A4}$$

From equation (A1), we can rewrite this as

$$\xi_s(\boldsymbol{r}) = \xi(\boldsymbol{r}) + \sum_{\boldsymbol{n}\neq(0,0,0)}^{\infty} \xi(\boldsymbol{r} - L\boldsymbol{n})\,. \tag{A5}$$

Applying this to the evolved linear power spectrum, which is isotropic, we arrive at the correction term, equation (5), to the correlation function for the periodic box:

$$\Delta\xi(\boldsymbol{r}) = \sum_{\boldsymbol{n}\neq(0,0,0)}^{\infty} - \xi_{\rm lin}(|\boldsymbol{r} + L\boldsymbol{n}|)\,. \tag{A6}$$

REFERENCES

Babul, A., & White, S. D. M. 1991, MNRAS, 251, 31
Bardeen, J. M., Bond, J. R., Kaiser, N., & Szalay, A. S. 1986, ApJ, 304, 15
Baugh, C. M. 1996, MNRAS, 280, 267
Baugh, C. M., & Efstathiou, G. 1993, MNRAS, 265,145
Baugh, C. M., & Gaztanaga, E. 1996, MNRAS, 280, 37
Bernardeau, F. 1994, ApJ, 433, 1
Bond, J. R., & Efstathiou, G. 1984, ApJ, 285, L45
———. 1991, Phys. Lett. B., 265, 245
Bouchet, F. R., Colombi, S., Hivon, E., & Juszkiewicz, R. 1995, A&A, 296, 575
Bower, R. G., Coles, P., Frenk, C. S., & White, S. D. M. 1993, MNRAS, 405, 403
Carlberg, R. G., & Couchman, H. M. P. 1989, ApJ, 340, 47
Carlberg, R. G., Couchman, H. M. P., & Thomas, P. A. 1990, ApJ, 352, L29
Carlberg, R. G., Yee, H. K. C., & Ellingson, E. 1997, ApJ, 478, 462
Cen, R., & Ostriker, J. P. 1992, ApJ, 399, 113
Centrella, J., & Melott, A. L. 1983, Nature, 305, 196
Cole, S. 1997, MNRAS, 286, 38
Cole, S., Weinberg, D. H., Frenk, C. S., & Ratra, B. 1997, MNRAS, 289, 37
Coles, P. 1993, MNRAS, 262, 1065
Colless, M. 1995, AJ, 109, 1937
Couchman, H. M. P., Pearce, F. R., & Thomas, P. A. 1996, preprint (astro-ph/9603116)
Couchman, H. M. P., Thomas, P. A., & Pearce, F. R. 1995, ApJ, 452, 797
Courteau, S., Faber, S. M., Dressler, A., & Willick, J. A. 1993, ApJ, 412, L51
Courant, R., & Hilbert, D. 1953, Methods of Mathematical Physics
Cray Research Inc. Cray MPP FORTRAN Reference Manual, SR-2504 6.1
Croft, R. A. C., & Efstathiou, G. 1994, MNRAS, 267, 390
Davis, M., Efstathiou, G., Frenk, C. S., & White, S. D. M. 1985, ApJ, 292, 371
Davis, M., & Peebles, P. J. E. 1983, ApJ, 267, 465
Dekel, A., & Rees, M. 1987, Nature, 326, 455
Dekel, A., et al. 1998, in preparation
Edge, A. C., Stewart, G. C., Fabian, A. C., & Arnaud, K. A. 1990, MNRAS, 245, 559
Efstathiou, G., Davis, M., Frenk, C. S., & White, S. D. M. 1985, ApJS, 57, 241
Efstathiou, G., & Eastwood, J. W. 1981, MNRAS, 194, 503
Efstathiou, G., Kaiser, N., Saunders, W., Lawrence, A., Rowan-Robinson, M., Ellis, R. S., & Frenk, C. S. 1990, MNRAS, 247, 10
Eke, V. R., Cole, S., & Frenk, C. S. 1996, MNRAS, 282, 263
Evrard, A. E. 1997, preprint (astro-ph/9701148)
Evrard, A. E., Summers, F. J., & Davis, M. 1994, ApJ, 422, 11
Fisher, K. B., Davis, M., Strauss, M. A., Yahil, A., & Huchra, J. P. 1994, MNRAS, 267, 927
Frenk, C. S. 1991, Models of Large Scale Structure, PhsS, 36, 70
Frenk, C. S., Evrard, A. E., White, S. D. M., & Summers, F. J. 1996, ApJ, 472, 460
Frenk, C. S., et al. 1998, in preparation
Frenk, C. S., White, S. D. M., & Davis, M. 1983, ApJ, 271, 471
Frenk, C. S., White, S. D. M., Efstathiou, G., & Davis, M. 1985, Nature, 317, 595
———. 1988, ApJ, 327, 507
———. 1990, ApJ, 351, 10
Fry, J., & Melott, A. 1985, ApJ, 292, 395
Garcia-Bellido, J., & Linde, A. 1997, CERN preprint (CERN-TH/97-08)
Gelb, J. M., & Bertschinger, E. 1994a, ApJ, 436, 467
———. 1994b, ApJ, 436, 491
Giovanelli, R. 1997, in The Extragalactic Distance Scale, ed. M. Liveo, M. Donohue, & N. Panagia (New York: Cambridge Univ. Press), in press
Górski, K. M., Ratra, B., Sugiyama, N., & Banday, A. J. 1995, ApJ, 444, L65
Gott, J. R., Turner, E. L., & Aarseth, S. J. 1979, ApJ, 234, 13
Groth, E. J., & Peebles, P. J. E. 1977, ApJ, 218, 592
Gunn, J., & Weinberg, D. 1995, in Wide Field Spectroscopy and the Distant Universe, ed. S. J. Maddox & A. Aragon-Salamanca (Singapore: World Scientific), 3
Guth, A., & Pi, S.-Y. 1981, Phys. Rev. Lett., 49, 1110
Hamilton, A. J. S., Kumar, P., Lu, E., & Matthews, A. 1991, ApJ, 374, L1
Henry, J. P. 1997, preprint
Henry, J. P., & Arnaud, K. A. 1991, ApJ, 372, 410
Jain, B., Mo, H. J., & White, S. D. M. 1995, MNRAS, 276, L25
Jenkins, A., et al. 1997, in Dark & Visible Matter in Galaxies & Cosmological Implications, ed. M. Persic & P. Salucci (city: publisher), 348
Jimenez, R., Thejll, P., Jorgensen, U. G., Macdonald, J., & Pagel, B. 1996, MNRAS, 282, 926
Jing, Y. P., Mo, H. J. & Börner, G. 1997, preprint (astro-ph/9707106)
Jing, Y. P., Mo, H. J., Börner, G., & Fang, L. Z. 1995, MNRAS, 276, 417
Kaiser, N. 1984, ApJ, 284, L9
Katz, N., Hernquist, L., & Weinberg, D. H. 1992, ApJ, 399, 109
Kennicutt, R. C., Freedman, W. L., & Mould, J. R. 1995, AJ, 110, 1476

Klypin, A. A., Primack, J., & Holtzman, J. 1996, ApJ, 466, 13
Klypin, A. A., & Shandarin, S. F. 1983, MNRAS, 204, 891
Lacey, C., & Cole, S. 1994, MNRAS, 271, 676
Lauer, T., & Postman, M. 1994, ApJ, 425, 418
Little, B., Weinberg, D. H., & Park, C. 1991, MNRAS, 253, 295
Lynden-Bell, D., Faber, S. M., Burstein, D., Davies, R. L., Dressler, A., Terlevich, R. J., & Wegner, G. 1988, ApJ, 326, 19
Maddox, S. J., Efstathiou, G., & Sutherland, W. J. 1996, MNRAS, 283, 1227
Maddox, S. J., Efstathiou, G., Sutherland, W. J., & Loveday, J. 1990, MNRAS, 242, 43P
Marzke, R. O., Geller, M. J., Da Costa, L. N., & Huchra, J. P. 1995, AJ, 110, 477
Mather, J. C., et al. 1990, ApJ, 354, L37
Melott, A. L., & Shandarin, S. F. 1993, ApJ, 410, 469
Mo, H. J., Jing, Y. P., & Börner, G. 1993, MNRAS, 264, 825
———. 1996, preprint (astro-ph/9607143)
Moore, B., Frenk, C. S., Efstathiou, G., & Saunders, W. 1994, MNRAS, 269, 742
Mould, J. R., Akeson, R. L., Bothun, G. D., Han, M., Huchra, J. P., Roth, J., & Schommer, R. A. 1993, ApJ, 409, 14
Padmanabhan, T. 1996, MNRAS, 278, 29P
Park, C. 1991, MNRAS, 251, 167
Park, C., Vogeley, M., Geller, M., & Huchra, J. P. 1994, ApJ, 431, 569
Peacock J. A., & Dodds, S. J. 1994, MNRAS, 267, 1020
———. 1996, MNRAS, 280, L19
Pearce, F. R., & Couchman, H. M. P. 1997, astro-ph/9703183
Pearce, F. R., Couchman, H. M. P., Jenkins, A. R., & Thomas, P. A. 1995, Hydra—Resolving a Parallel Nightmare, in Dynamic Load Balancing on MPP systems
Peebles, P. J. E. 1980, The Large Scale Structure of the Universe (Princeton: Princeton Univ. Press)
———. 1982, ApJ, 263, L1
Postman, M., & Lauer, T. 1995, ApJ, 440, 28
Ratcliffe, A., Shanks, T., Parker, Q. A., & Fong, R. 1997, preprint (astro-ph/9702227)
Ratra, B., Sugiyama, N., Banday, A. J., & Górski 1997, ApJ, 481, 22
Renzini, A., et al. 1996, ApJ, 465, L23
Richstone, D. O., Loeb, A. A., & Turner, E. L. 1992, ApJ, 393, 477
Saglia, R. P., Bertschinger, E., Baggley, G., Burstein, D., Colless, M., Davies, R. L., McMahan, R. K., & Wegner, G. 1997, ApJS, 109, 79
Saunders, W., Rowan-Robinson, M., Lawrence, A., Efstathiou, G., Kaiser, N., Ellis, R. S. E., & Frenk, C. S. 1990, MNRAS, 242, 318
Seljak, U., & Zaldarriaga, M. 1996, ApJ, 469, 437
Shectman, S. A., Landy, S. D., Oemler, A., Tucker, D. L., Lin, H., Kirshner, R. P., & Schechter, P. L. 1996, ApJ, 470, 172
Smith, C. C., Klypin, A., Grossman, M. A. K., & Holtzman, J. 1997, preprint (astro-ph 970209)
Smoot, G., et al. 1992, ApJ, 396, L1
Sommerville, R., Davis, M., & Primack, J. R. 1997, ApJ, 479, 606
Tadros, H., & Efstathiou, G. 1995, MNRAS, 276, 45
———. 1996, MNRAS, 282, 138
Thomas, P. A., et al. 1997, preprint (astro-ph/9707018)
Tormen, G. 1996, preprint (astro-ph/9611078)
Tucker, D. L., et al. 1997, MNRAS, 285, L5
Tytler, D., Fan, X.-M., & Burles, S. 1996, Nature, 381, 207
Viana, P. T. P., & Liddle, A. R. 1996, MNRAS, 281, 323
Vogeley, M. S., Park, C., Geller, M. J., & Huchra, J. P. 1992, ApJ, 391, 5
Weinberg, D. H. 1995, A&AS, 186, 2902
Weinberg, D. H., & Cole, S. 1992, MNRAS, 259, 652
White, D. A., & Fabian, A. C. 1995, MNRAS, 273, 72
White, M., Gelmini, M., & Silk, J. 1995, Phys. Rev. D, 51, 2669
White, S. D. M. 1996, in Cosmology and Large-Scale Structure, ed. R. Schaefer, J. Silk, M. Spiro, & J. Zinn-Justin (Dordrecht: Elsevier)
White, S. D. M., Davis, M., Efstathiou, G., & Frenk, C. S. 1987a, Nature, 330, 451
White, S. D. M., Davis, M., & Frenk, C. S. 1983, MNRAS, 209, 27P
White, S. D. M., Efstathiou, G., & Frenk, C. S. 1993, MNRAS, 262, 1023
White, S. D. M., Frenk, C. S., & Davis, M. 1983, ApJ, 274, L1
White, S. D. M., Frenk, C. S., Davis, M., & Efstathiou, G. 1987b, ApJ, 313, 505
White, S. D. M., Navarro, J. F., Evrard, A. E., & Frenk, C. S. 1993, Nature, 366, 429
Willick, J. A., Courteau, S., Faber, S. M., Burstein, D., Dekel, A., & Strauss, M. A. 1997, ApJS, 109, 333
Zeldovich, Ya. B. 1970, A&A, 5, 84
Zurek, W. H., Quinn, P. J., Salmon, J. K., & Warren, M. S. 1994, ApJ, 431, 559